Knockdown of the CXCL12/CXCR7 chemokine pathway results in learning deficits and neural progenitor maturation impairment in mice

Françoise Trousse, Achraf Jemli, Michèle Silhol, Elisabeth Garrido, Lucie Crouzier, Gaëlle Naert, Tangui Maurice, Mireille Rossel

Knockdown of the CXCL12 /CXCR7 chemokine pathway results in learning deficits and neural progenitor maturation impairment in mice

Trousse Françoise[a], Jemli Achraf[a,b], Silhol Michèle[a], Garrido Elisabeth[a], Crouzier Lucie[a], Naert Gaëlle[a], Maurice Tangui[a], Rossel Mireille[a,*]

[a] MMDN, Univ. Montpellier, EPHE, INSERM, UMR-S1198, PSL Research University, Montpellier, France

[b] Lab. Genetics, Biodiversity and Bioresources valorization (LR11ES41), Higher Institute of Biotechnology of Monastir, University of Monastir, Monastir, Tunisia

[*] Corresponding author: Mireille Rossel. Tel.: +33 4 67 14 38 15

E-mail addresses: Françoise Trousse <francoise.trousse@umontpellier.fr>, Jemli Achraf <jemliiachraf@yahoo.fr>, Michelle Silhol michelle_silhol@orange.fr, Elisabeth Garrido <elisabethgarrido66@gmail.com>, Lucie Crouzier <lucie.crouzier@umontpellier.fr>, Gaëlle Naert <gaelle.naert@cilcare.com>, Tangui Maurice <maurice@univ-montp2.fr>, Mireille Rossel <mireille.rossel@umontpellier.fr>.

Keywords

CXCL12 knockdown mice; CXCR7 knockdown mice; AMD3100; behavioral and learning deficits; adult hippocampal neurogenesis; expression of immediate-early genes (IEGs) in neuronal excitability

Highlights

- CXCR7 and CXCL12 knockdowns result in learning and memory deficits.
- CXCR7 downregulation leads to impairment of the CXL12-CXCR4 signaling pathway.
- Defect of precursor cell proliferation in dentate gyrus is linked to decreased CXCR4-CXCL12 expression.

- CXCR7 knockdown results in failure of newborn neuron differentiation in the hippocampus.

Abbreviations

ACKR3, atypical chemokine receptor 3**;** AD, Alzheimer disease; BDNF, Brain derived neurotrophic factor; DCX, doublecortin; DG, dentate gyrus; IP, intraperitoneally; GCL, granular cell layer; KD, knockdown; KPBS, potassium phosphate buffer saline; IEG, immediate-early gene; O, other quadrants; RT, reverse transcription; SGZ, sub-granular zone; T, training quadrant; TLP, temporal lobe epilepsy; WT, wild type.

Abstract

In adult brain, the chemokine CXCL12 and its receptors CXCR4 and CXCR7 are expressed in neural progenitor and glial cells. Conditional *Cxcl12* or *Cxcr4* gene knockout in mice leads to severe alterations in neural progenitor proliferation, migration and differentiation. As adult hippocampal neurogenesis is involved in learning and memory processes, we investigated the long-term effects of reduced expression of CXCL12 or CXCR7 in heterozygous *Cxcl12*$^{+/-}$ and *Cxcr7*$^{+/-}$ animals (KD mice) on hippocampal neurogenesis, neuronal differentiation and memory processing. In *Cxcl12* KD mice, *Cxcr4* mRNA expression was reduced, whereas *Cxcr7* was slightly increased. Conversely, in *Cxcr7* KD mice, both *Cxcr4* and *Cxcl12* mRNA levels were decreased. Moreover, *Cxcl12* KD animals showed marked behavioral and learning deficits that were associated with impaired neurogenesis in the hippocampus. Conversely, *Cxcr7* KD animals showed mild learning deficits with normal neurogenesis, but reduced cell differentiation, measured with doublecortin immunolabeling. These findings suggested that a single *Cxcl12* or *Cxcr7* allele might not be sufficient to maintain the hippocampal niche functionality throughout life, and that heterozygosity might represent a susceptibility factor for memory dysfunction progression.

1. Introduction

The chemokine CXCL12 and its receptors CXCR4 and CXCR7 (also called atypical chemokine receptor 3**,** ACKR3) are widely expressed in the developing and adult nervous system of mice and humans (Schönemeier et al., 2008; Stumm et al., 2003; Tiveron et al., 2010; Trousse et al., 2015; Shimizu et al., 2011). The CXCL12/CXCR4 axis activity is an essential triggering signal for different neural progenitor cell functions, including survival, proliferation and migration. In adult brain, the CXCL12/CXCR4 axis is a major signaling pathway during hippocampal neurogenesis within the molecular layer of the dentate gyrus (DG) (Schultheiß et al., 2013). Recent data showed that CXCR7 plays an important role in CXCL12-mediated cell cycle regulation and proliferation of neural precursor cells (Abe et al., 2018; Wang et al., 2016). However, CXCR7 functions in the adult hippocampus, particularly its role in neural precursor survival, maturation and network connection, remain to be clarified because it has been suggested that it could act as a regulator of CXCR4 expression/function (Sánchez-Alcañiz et al., 2011; Shimizu et al., 2011). CXCR7 was first considered to be a scavenger receptor, but CXCR4-independent functions have been recently described (Chen et al., 2015). In physiological as well as tumoral conditions, CXCR4 and CXCR7 were found to elicit independent processes. For instance, a study on oligodendrocyte development showed that CXCR4 inhibition reduces CXCL12 beneficial effects on proliferation and migration of oligodendrocyte progenitor cells, while CXCR7 knockdown hinders their differentiation (Yuan et al., 2018). CXCR4 expression is regulated by CXCR7 during interneuron development (Wang et al., 2011). Moreover, *Cxcl12*$^{-/-}$ and *Cxcr7*$^{-/-}$ knockout embryos show a comparable phenotype during Cajal-Retzius cell development (Trousse et al., 2015). Therefore, CXCR7 may play a major role in regulating the CXCL12/CXCR4/CXCR7 interactions.

CXCL12 chemokine signaling is strongly decreased in patients with Alzheimer's disease (AD) and in transgenic mouse models of AD with impaired memory functions (Laske et al., 2008; Parachikova and Cotman, 2007). Moreover, pharmacological inactivation of CXCR4 results in memory deficits similar to those observed in mouse AD models (Parachikova and Cotman, 2007). Conversely, CXCR7 role in this

context remains unexplored.

We therefore used heterozygous *Cxcl12* and *Cxcr7* knockdown (KD) mice (Trousse et al., 2015) to investigate the effect of *Cxcl12* and *Cxcr7* downregulation on their learning capacities and hippocampal neurogenesis. We observed functional alterations in learning and memory processes as well as in plasticity gene regulation and abnormal neural stem cell maturation during adult neurogenesis in both *Cxcl12* and *Cxcr7* KD animals. This suggests that alterations of the CXCL12/CXCR7 pathways may play an important role in pathological aging.

2. Materials and methods

2.1. Animals

Cxcl12$^{+/-}$ mice were described previously (Nagasawa et al., 1996). *Cxcr7* floxed mice were generated at the Mouse Clinical Institute (Illkirch, France). Exon 2, which contains the entire coding region, was flanked by loxP sites and the obtained *Cxcr7* floxed mice were then backcrossed with C57BL/6J animals (Charles River, France), as described previously (Trousse et al., 2015). The heterozygous *Cxcr7*$^{+/Fl}$ progeny was crossed with CMV-Cre deleter mice to obtain *Cxcr7*$^{+/-}$ males and females (Schwenk et al. 1995). For behavioral and biochemical experiments, 3-8-month-old heterozygous mice (KD throughout the study) were used. Male Swiss CD-1 mice were from Janvier (Saint-Doulchard, France). They were used at 9 weeks of age. Animals were housed in the University of Montpellier animal facility (agreement from the French Ministry of Agriculture D34-172-23), in groups of 10 individuals in 48 cm x 27 cm cages (940 cm^2 floor area, Techniplast) with *ad libitum* access to food and water. They were kept in a temperature and humidity controlled facility with a 12h/12h light/dark cycle (lights on at 7.00 am). Behavioral experiments were carried out between 9.00 am and 5.00 pm in a sound-attenuated and air-regulated experimental room after a habituation period of 30 min. All animal procedures were performed in strict adherence to the European Union directive 2010/63 and the ARRIVE guidelines (Kilkenny et al., 2010).

2.2. Drug and administration procedure

1,1-[1,4-Phenylenebis(methylene)]bis-1,4,8,11-tetraazacyclotetradecane octahydrochloride (AMD3100; Sigma-Aldrich, Saint-Quentin-Fallavier, France) was solubilized in physiological saline and intraperitoneally injected (1 or 3 mg/kg) in male Swiss mice once per day for 4 days. Control mice received saline solution.

2.3. Behavioral assays

In a preliminary experiment, spontaneous alternation in the Y-maze test, a spatial working memory measure, was evaluated in a first cohort of WT (n = 6 males and n = 6 females) and *Cxcl12* KD (n = 7

males and n = 4 females) and of WT (n = 11 males and n = 10 females) and *Cxcr7* KD (n = 2 males and n = 6 females) mice (Fig. 1a). Then, spontaneous alternation and place learning in the water-maze test, a spatial reference long-term memory measure, were assessed in a second cohort of WT (n = 5 males and n = 7 females) and *Cxcl12* KD (n = 11 males and n = 8 females) and of WT (n = 5 males and n = 5 females) and *Cxcr7* KD (n = 10 males and n = 10 females) mice (Fig. 1b). Alternation data from the two cohorts were pooled *a posteriori*. Both tests are spatial learning tests that are largely hippocampus-dependent and likely influenced by neurogenesis dynamics (for reviews, see (Abrous and Wojtowicz, 2015, Lieberwirth et al., 2016). Indeed, spatial learning enhances neurogenesis (Gould et al., 1999; Trouche et al., 2009), while reduced neurogenesis (due to ageing or experimental low dose irradiation of the hippocampus) is linked to learning impairment in the water-maze and T-maze alternation (Madsen et al., 2003; Raber et al., 2004; Snyder et al., 2005; van Praag et al., 2005).

For the pharmacological experiment with AMD3100 (Fig. 1c), Swiss CD-1 male mice were used because they are good learners in control conditions and prone to learning alterations in pathological conditions (Phan et al., 2002)). Two complementary tests were performed to evaluate spatial working memory (spontaneous alternation) and long-term non-spatial memory (passive avoidance) and to obtain the most information with a limited injection protocol. Mice were treated or not with AMD3100 (n = 9-10/group) once per day starting 2 days before the behavioral tests (Fig. 1c). On test day, mice received the AMD3100 injection 20 min before the Y-maze test session (day 3) and before passive avoidance training (day 4). Retention was analyzed after 24 h without any further drug treatment (Fig. 1c).

2.4. Spontaneous alternation in the Y-maze

The spontaneous alternation performance in the Y-maze was used as a spatial working memory index (Maurice, 2016; Maurice et al., 1994a, 1994b). The Y-maze was made of grey PVC and each arm was 40 cm long, 13 cm high, 3 cm wide at the bottom, 10 cm wide at the top, and converged at an equal angle. Each mouse was placed at the end of one arm and allowed to move freely through the maze during an 8min session. Arm entries were visually monitored. They were validated when the animal placed all four

paws in the arm and included possible returns into the same arm. An alternation was defined as entries into all three arms on consecutive occasions. Therefore, the maximum number of alternations was the total number of arm entries minus two, and the alternation percentage was calculated as follows: actual alternations / maximum alternations x 100. Parameters included the alternation percentage (memory index) and the total number of arm entries (exploration index). Animals that performed less than 8 arm entries in 8 min or with an alternation percentage < 20% or > 90% were discarded from the analysis. Attrition was 4.3% in this study.

2.5. Place learning in the water-maze

Spatial reference memory was evaluated using platform location learning in a circular pool (diameter 140 cm, height 40 cm) (Maurice, 2016; Rodríguez Cruz et al., 2017). The water temperature (23 ± 1°C), light intensity, external cues in the room, and water opacity were rigorously reproduced. A transparent Plexiglas non-slippery platform (diameter: 10 cm) was immersed under the water surface during the acquisition step. Swimming was recorded using the Videotrack software (Viewpoint, Lissieu, France), and trajectories were analyzed as latencies and distances. The software divided the pool in four quadrants, with the platform set in the middle of one quadrant.

Acquisition. Training consisted in 3 swims per day for 5 days, with 20 min interval between trials. Start positions, set at the limits between quadrants, were randomly selected and each animal was allowed a 90s swim to find the platform. The platform location was changed every day. The time required to find the platform (swimming latency) was measured using a stopwatch. Animals were left on the platform for 20 s. Animals that did not find the platform after 90s were placed on it manually and left for 20 s. The median latency was calculated for each training day and expressed for the experimental group as the mean ± SEM. Acquisition slopes, calculated individually by linear regression of the median swimming duration, were analyzed individually.

Retention. A probe test was performed 24h after the last acquisition session. The platform was removed and each animal was allowed a free 60 s swim. The start position for each mouse was one of

the two start positions located away from the platform location in alternating order. The swim was video-tracked and the swimming speed and time spent in the training (T) and other (o) quadrants was quantified. No exclusion criterion was set for this test.

2.6. Passive avoidance test

In AMD3100-treated mice, non-spatial long-term memory was evaluated using a one-trial acquisition passive avoidance test (Maurice, 2016). The apparatus was a two-compartment (15 × 20 × 15 cm high) box in which one compartment was illuminated and with white polyvinylchloride walls and the other dark and with black polyvinylchloride walls and a grid floor. A guillotine door separated the two compartments. A 60 W lamp positioned 40 cm above the apparatus illuminated the white compartment during the experiment. Scrambled foot shocks (0.3 mA for 3 s) could be delivered to the grid floor using a shock generator scrambler (Lafayette Instruments, Lafayette, USA). The guillotine door was initially closed during the training session. Each mouse was placed in the white compartment. After 5s, the door was raised. When the mouse entered the darkened compartment and placed all four paws on the grid floor, the door was closed and scrambled foot shocks delivered for 3s. The step-through latency, i.e., the latency spent to enter the darkened compartment, and the numbers of vocalizations were recorded. The retention test was carried out 24h after training. Each mouse was placed again in the white compartment, and after 5s, the door was raised. The step-through latency was recorded up to 300s (Maurice, 2016). No exclusion criterion was set for this test.

2.7. Animal sacrifice and sample preparation

After the last behavioral session, mice were anesthetized and transcardially perfused with 0.9% NaCl. Half brain was rapidly removed from the skull and the hippocampus was dissected and rapidly frozen in liquid nitrogen and stored at -80°C for mRNA analysis. The other half brain was fixed in 4% paraformaldehyde, pH 9.5, at 4°C for 2–4 days, and then placed in paraformaldehyde solution containing 10% sucrose at 4°C overnight.

2.8. RNA extraction and reverse transcription (RT)

Total RNA was extracted from the hippocampus using the NucleoSpin R 8/96 RNA kit (Macherey-Nagel, Germany) according to the manufacturer's instructions, including incubation with DNase at room temperature for 25 min. RNA concentration and quality were evaluated with the Agilent RNA 6000 Nano Kit (Agilent Technologies, Waldbronn, Germany). cDNA was synthesized in a 20 µl reaction mixture in which 1 µg of total RNA was mixed with 1 µl of random hexamer primer (0.5 µg/µl) (Amersham, Orsay, France) and then incubated at 70 °C for 10 min. After cooling on ice, the solution was mixed with 4 µl 5X first strand buffer, 2 µl of 0.1 M DTT, 1 µl each of dATP, dTTP, dCTP, dGTP (10 mM/each) and 1 µl MuMLV reverse transcriptase (200 U; Promega, Charbonnieres, France) and incubated at 37°C for 60 min, followed by 70°C for 15 min. Concomitantly, an aliquot of each RNA sample was incubated in the absence of MuMLV to assess the degree of genomic DNA contamination. RT samples were stored at −20 °C until use (Arancibia et al., 2008).

2.9. Quantitative Real-Time PCR

For each sample, real-time PCR was performed in triplicate using a LightCycler 480 Instrument (Roche Diagnostics, Mannheim, Germany) according to the manufacturer's instructions; data were from four independent experiments for each group. PCR reactions were performed in a final volume of 6 µl that included 1 × LC-DNA Master SYBR Green I mix, 1 µM of each primer and 1/25 diluted RT mixture added as PCR template (water was used as negative control). Amplification conditions were: (i) cDNA denaturation (1 cycle: 95°C for 10 min); (ii) amplification (45 cycles: denaturation at 95°C for 10 s, annealing at 60°C for 10 s, elongation at 72°C for 10 s); (iii) melting curve analysis (one cycle from 65°C to 95°C for 60 s); (iv) cooling (one cycle: 40°C for 60 s). Real-time detection of SYBR Green I fluorescence intensity, which indicates the amount of PCR product formed, was measured at the end of each elongation phase. Threshold cycles for each target gene in control and KD hippocampus samples were determined by using the housekeeping actin gene, *Actb,* as normalization control. Primers are listed in Supplementary Table 1.

2.10. Tissue analysis

Frozen half brains were mounted on a microtome (Microm HM 450, Thermo Fisher) and 25 µm coronal sections were cut. Sections were collected in cold cryoprotectant solution (0.05 M sodium phosphate buffer, pH 7.3, 30% ethylene glycol, and 20% glycerol) and stored at -20°C until immunocytochemistry (Naert and Rivest, 2011).

2.11. Immunohistochemistry

Every 12th brain section, starting from the olfactory bulb to the end of the cerebral cortex, was mounted on Colorfrost/Plus microscope slides (Thermo Fisher Scientific) for *Cxcl12*$^{+/-}$, *Cxcr7*$^{+/-}$ and WT mice (3–8 months of age; n = 10-20 per group). Localization of Ki67, SOX2, Doublecortin (DCX), IBA1 and GFAP was evaluated by immunohistochemistry as reported previously (Nadeau and Rivest, 2000). Briefly, sections were washed in potassium phosphate buffer saline (KPBS) and were blocked with a solution containing KPBS, 0.4% Triton X-100, 4% normal goat serum, and 1% bovine serum albumin (KPBS permeabilizing solution) for 30 min. Then, they were incubated (at 4°C overnight) with rabbit anti-Ki67 (dilution 1:100, ab16667, Abcam), mouse anti-SOX2 (dilution 1:50, ab20J5, Abcam), rabbit anti-DCX (dilution 1:500, 4604S, Cell Signaling), rabbit anti-GFAP (dilution 1:500, Z0334, Dako), and anti-rabbit-IBA1 (dilution 1:500, Wako Chemicals GmbH, Neuss, Germany) primary antibodies (diluted 1:1 in KPBS:KPBS permeabilizing solution). The anti-Ki67 antibody was added after the antigen retrieval step in citrate buffer/10% glycerol (10 mM, pH 6) at 65°C for 1 h. After several washes, sections were incubated with biotinylated goat anti-rabbit or anti-mouse secondary antibodies (dilution 1:200, BA-1000 and BA-9200 respectively, Vector laboratories) for 2h followed by the avidin–biotin–peroxidase complex (Vectastain ABC Elite Kit; Vector Laboratories) and detection with 0.05% 3,3-diaminobenzidine tetrahydrochloride and 0.003% hydrogen peroxide. After dehydration through successive alcohol baths, all sections were stained with Cresyl violet and mounted with mounting medium (Mountex). Positive cells in the granular cell layer (GCL) and sub-granular zone (SGZ) of the DG were manually counted using an optical

microscope (DM 2500, Leica) under white light at x40 magnification. The number of Ki67, SOX2 or DCX positive cells in each hippocampus was determined by combining the cell counts per section (at least 5 sections/animal), and per DG area (cells/mm^2). For GFAP and IBA1 staining, the DG area was quantified by measuring the staining intensity after the background was subtracted, using the ImageJ software. A global threshold was applied for intensity measurement. Values were expressed as the mean ± SEM normalized to the surface unit (in μm^2) and expressed as the percentage of the control mean value. All quantifications were performed by an experimenter blind to the experimental conditions.

2.12. Statistical analyses

Data were expressed as the mean ± SEM, but for the passive avoidance latencies that are non-parametric data because an upper cut-off time was set and were expressed as median and interquartile range. Data were analyzed using one-way ANOVA (*F* values), followed by the Dunnett's *post hoc* multiple comparison test for parametric data or Kruskal-Wallis ANOVA followed by a Dunn's test for non-parametric data. Acquisition profiles in the water-maze were analyzed using the non-parametric repeated-measure Friedman's ANOVA (*Fr* value), followed by the Mann-Whitney's test for the different groups. Probe test data were compared to the 15s level using the one-sample *t*-test. For qPCR quantification and cell counting, group comparisons were performed with the unpaired t-test. When ANOVA values were < 1, the probability could not reach significance whatever the degrees of freedom. Therefore, they were indicated as $F < 1$. The level of statistical significance was set at $p < 0.05$. For clarity, all statistical data were included in the figure legends.

3. Results

3.1. Cxcr7 KD causes a strong downregulation of Cxcr4/Cxcl12 expression

During development and adult life, the expression of *Cxcl12*, *Cxcr4*, and *Cxcr7* is highly regulated in the hippocampus (Abe et al., 2018; Banisadr et al., 2015; Stumm et al., 2003). As these three genes are expressed concomitantly at all stages, and given that chemokines can regulate their receptor expression, we first analyzed their expression in the hippocampus of adult *Cxcl12* KD and *Cxcr7* KD mice by RT-qPCR. We considered only heterozygous animals because *Cxcl12*$^{-/-}$ and *Cxcr7*$^{-/-}$ mice are not viable (Trousse et al., 2015). In *Cxcl12* KD mice, *Cxcl12* mRNA expression was significantly decreased by 26% and *Cxcr4* mRNA levels by 12% compared with WT littermates. Conversely, *Cxcr7* mRNA level was slightly, not significantly increased by +13% (Fig. 2a).

On the other hand, in adult *Cxcr7* KD mice, C*xcr7* mRNA level was strongly reduced (-59%; Fig. 2b), indicating that a single allele could not maintain the expression level. *Cxcl12* (-49%) and *Cxcr4* (-46%) also were similarly downregulated compared with WT littermates (Fig. 2b). These findings confirmed that in *Cxcr7* KD animals, CXCR7 regulates the expression of C*xcr4* and *Cxcl12*, as previously reported (Liu et al., 2018; Sánchez-Alcañiz et al., 2011). They also indicated that in adult *Cxcr7* KD mice, the CXCL12 signaling pathway is more affected because the expression of all three partners was reduced.

3.2. Impaired learning and memory in Cxcl12 KD and Cxcr7 KD animals

As reduced CXCL12/CXCR4 signaling is associated with learning deficits (Laske et al., 2008; Parachikova and Cotman, 2007), we investigated the learning and memory performances of *Cxcl12* KD mice and WT littermates (males and females). First, we evaluated the spatial working memory using the spontaneous alternation behavior in the Y-maze, as described in Figure 1. Alternation was significantly reduced in *Cxcl12* KD male and female, indicating major working memory deficits (Fig. 3a). In terms of locomotion, WT and *Cxcl12* KD female mice tended to enter more arms during the session compared with males (Fig. 3b). We then analyzed the spatial reference memory using the place learning task in the water-maze. In both WT and *Cxcl12* KD male (Fig. 3c) and female (Fig. 3d) animals, the swimming latency to find the

platform decreased during the training trials. However, analysis of the acquisition slopes showed that the acquisition efficacy was significantly reduced in *Cxcl12* KD mice (both sexes) with a diminution of the swimming latency of 11-15 s per trial in *Cxcl12* KD and of 18-21 s in WT mice (Fig. 3e). The probe test, performed without platform, showed that *Cxcl12* KD mice swam slightly albeit significantly faster than WT animals (both sexes) (Fig. 3f), but failed to preferentially explore the T quadrant, differently from WT animals (both sexes) (Fig. 3g). Finally, we assessed the spatial working memory by changing the platform location in the water-maze each day during the training sessions. Swimming performances were analyzed by calculating the acquisition slopes across swimming trials (Fig. 3h). Working memory was significantly reduced in *Cxcl12* KD mice (both sexes), confirming the results obtained with the spontaneous alternation test. These findings indicate that *Cxcl12* KD mice present significant alterations of learning and of short-term and long-term memory processes, independently from their sex.

Then, we evaluated *Cxcr7* KD mice using the same behavioral tests (Fig. 4). Alternation behavior in the Y-maze was significant reduced in *Cxcr7* KD mice compared with WT littermates (Fig. 4a), particularly in females. The two-way ANOVA indicated that female WT and KD mice tended to enter more arms during the 8-min session than males, but no group difference was measured using the *post-hoc* test (Fig. 3b). In the water-maze test, swimming duration to find the platform progressively decreased in *Cxcr7* KD and WT males (Fig. 4c) and females (Fig. 4d) during the training sessions, although during session 5, this time was significantly longer in *Cxcr7* KD than in WT males (Fig. 4c). However, the analysis of the acquisition slopes did not highlight any difference between WT and *Cxcr7* KD mice (Fig. 4e). Similarly, swimming speed during the probe test was comparable between groups (Fig. 4f). On the other hand, *Cxcr7* KD mice (both sexes) failed to preferentially explore the T quadrant, differently from WT animals (Fig. 4g). The swimming performances during spatial working memory test, based on the daily change of the platform location were analysed. The acquisition slopes (Fig. 4h) indicated that performances was significantly reduced in *Cxcr7* KD mice (both sexes) compared with WT animals, confirming the spontaneous alternation results. These findings indicate that learning and memory are affected also in *Cxcr7* KD mice.

Finally, we examined learning and memory abilities of mice after a pharmacological blockade of the CXCR4 pathway (Fig. 5). We evaluated learning and memory in Swiss CD-1 male mice treated with the CXCR4 antagonist AMD3100 (1 and 3 mg/kg) for 3 days before the spontaneous alternation task or for 4 days before the non-spatial long-term memory analysis using a one-trial passive avoidance task (Fig. 1c). Alternation performance was significantly reduced in mice treated with AMD3100 (both doses) compared with controls (vehicle) (Fig. 5a), without affecting the number of arms entered during the 8 min session (Fig. 5b). In the passive avoidance test, the step-though latency was only significantly reduced in mice treated with 3 mg/kg AMD3100 (Fig. 5c), whereas escape latency tended to increase (not significant) (Fig. 5d). These data show that acute blockade CXCR4 receptors also impaired learning and memory.

3.3. Impact of Cxcr7/Cxcl12 gene expression deregulation on brain plasticity

We next measured the expression of three immediate-early genes (IEGs) related to memory and hippocampal/neuronal excitability, namely *c-Fos, Arc*, *Egr*1 (Guzowski et al., 2001), and the *Creb1* transcriptional activator (Lopez de Armentia et al., 2007) in KD animals and WT littermates. Since animals underwent long-term training and behavioural examination, we measured only IEGs levels 24h after the last behavioral session, *i.e.*, back to basal levels but not the transient increase of the levels after an acute stimulus, in the different mouse models. Indeed, transcriptional dysfunctions resulting in altered basal levels of IEGs have been observed in mouse models with impaired memory (Christensen et al., 2013). In *Cxcl12* KD mice, expression of *c-Fos* and *Egr1* was significantly increased compared with WT littermates (+24%, $p < 0.01$ for *c-Fos* and +7%, $p < 0.05$ for *Egr1*; Fig. 6a), suggesting high neuronal excitability. Conversely, *Creb1* level was decreased (-10%, $p < 0.05$; Fig. 6a). The expression of the post-synaptic protein *Arc* also was upregulated (+25%, $p < 0.001$) in *Cxcl12* KD compared with WT mice suggesting increased neuronal activity associated with memory retention (Tzingounis and Nicoll, 2006). Such increase might not be sufficient to compensate the learning defects in *Cxcl12* KD animals.

In *Cxcr7* KD animals, *c-Fos* (-23%, $p > 0.05$) and *Creb1* (-25%, $p < 0.01$) were downregulated (Fig. 6b), suggesting a dysregulation of neuronal activity consistent with the observed behavioral defects.

Conversely, *Arc* and *Egr1* were comparable in *Cxcr7* KD and WT mice suggesting no alteration of synaptic activity.

3.4. Impaired hippocampal neurogenesis in Cxcl12 and Cxcr7 KD mice

As CXCR4/CXCL12 signaling is necessary for neuronal progenitor pool maintenance and proper cell dispersion in the adult DG dentate gyrus (Schultheiß et al., 2013), , we analyzed neurogenesis in KD animals to determine the cellular mechanisms involved in the observed learning deficits. Using precursor cell markers (Ki67 and SOX2), we analyzed the hippocampal neural progenitor pool within the DGdentate gyrus, and quantified the progenitor number and position in SGZ and GCL. The number of Ki67-positive cells in the SGZ was slightly decreased in *Cxcl12* KD mice (38.4 ± 5.7 cells/mm^2 vs 60.4 ± 8.6 cells/mm^2 in WT, $p < 0.05$; Fig. 7a-b', and m) without any major ectopic cell location, and was unchanged in *Cxcr7* KD mice (49.9 ± 8.6 cells/mm^2, not significant; Fig. 7g-h', and m). In both mutants, the total number of SOX2-expressing cells was comparable with that of WT controls (Fig. 7c-d', i-j', and n). Nevertheless, the number of SOX2-positive cells located in the GCL was higher in *Cxcr7* KD than in WT littermates (Supplementary Fig. 1a).

We then assessed the expression of DCX, a marker of proliferating neuroblasts and immature and differentiated neurons (von Bohlen und Halbach, 2011), to determine whether mutant mice had defects in maturation and differentiation of hippocampal neurons. We did not detect any difference between *Cxcl12* KD and WT samples. Conversely, the total number of DCX-positive cells was significantly reduced in *Cxcr7* KD mice (281.2 ± 45.2 vs 533.6 ± 77.2 cells/mm^2 in WT, $p < 0.01$, Fig. 7e-f, k-l, and o). This reduction concerned neuroblasts, i.e., DCX-positive cells with small or no process and exclusively located in the SGZ (Ables et al., 2010) (111.9 ± 18.3 in *Cxcr7* KD vs 173.9 ± 35.8 cells/mm^2 in WT, not significant, Supplementary Fig. 1b), and particularly immature neurons, i.e., DCX-positive cells with process extending through the GCL (109.9 ± 23.2 in *Cxcr7* KD vs 242.4± 52.9 cells/mm^2 in WT, $p < 0.05$). Moreover, in *Cxcr7* KD mice, fewer DCX-positive neurons were present in the DG depth with fewer branching dendrites compared with WT littermates (Supplementary Fig. 2).

This decrease was not associated with increased cell death analyzed by cleaved caspase3 immunolabeling (data not shown). On the other hand, the higher number of DCX-positive neuroblasts and the lower number of DCX-positive immature neurons in *Cxcr7* KD than in WT mice ($p < 0.05$, Supplementary Fig. 1c) suggested a differentiation defect.

3.5. Assessment of glial activation in the hippocampus of Cxcl12 KD and Cxcr7 KD mice

A dysfunction of the chemokine axis might results in deregulation of the glial environment with modifications of the astrocyte or microglia migration properties because CXCR4 and CXCR7 are expressed in astrocytes and microglia. To determine whether astrogliosis and microglial activation were affected in in *Cxcl12* KD and *Cxcr7* KD mice, we quantified GFAP and IBA1 staining intensity within the hippocampus (Fig. 8a-j). In *Cxcl12* KD mice, GFAP (+53%; not significant, Fig. 8i) and IBA1 (+86%, $p < 0.05$) signal intensity was higher than in WT controls (Fig. 8j). Conversely, it was comparable in *Cxcr7* KD and WT samples. Altogether, our data suggest that microglia activation might occur in *Cxcl12* KD.

4. Discussion

4.1. Knockdown mice as a model of chemokine pathway alterations

Chemokines play a major role in cell differentiation and adult hippocampal neurogenesis, from neural stem cells to mature granular neurons, via progenitor cells and newborn neurons (Abe et al., 2018; Schultheiß et al., 2013; Wang et al., 2016). As neurogenesis may sustain active learning and memory processes, particularly long-term memory, we investigated the effect of impairing the CXCL12/CXCR4 and CXCL12/CXCR7 pathways on brain plasticity, IEG expression, hippocampal neurogenesis and learning and memory abilities.

To this aim, we used heterozygous *Cxcl12* and *Cxcr7* KD animals that represent the closest physiological model of expression knockdown in key brain structures involved in neurodegenerative pathologies such as the hippocampal formation. In *Cxcl12* KD mice, decreased *Cxcl12* expression was associated with significant *Cxcr4* mRNA reduction and learning and memory task impairment. We also observed that after pharmacological inhibition of CXCR4 signaling, memory retention was altered in treated animals. Conversely, *Cxcr7* expression was only slightly increased in *Cxcl12* KD mice. On the other hand, in *Cxcr7* KD mice, *Cxcr4* and *Cxcl12* were both strongly downregulated in the hippocampus, close to 50% of the levels in WT animals. Such decrease was unexpected because a transcriptional regulation of chemokine expression by CXCR7 was never reported before. Indeed, a previous study showed that CXCR7 downregulation leads to an increase of extracellular CXCL12 levels, which in turn trigger CXCR4 endocytosis and degradation with defects in CXCR4-mediated functions (Sanchez-Alcaniz et al., 2011). Together with our findings, this is convincing evidence that *Cxcr7* maintains a stable expression level of *Cxcr4* and ensures its sensitivity to CXCL12. Moreover, expression of CXCR4 enhances the recruitment of CXCR7 by β-arrestin and reduces the affinity of CXCL12 for CXCR7. Thus, CXCR4 and CXCR7 seem to be kept in balance by mutually regulating their expression and signaling pathways (Cheng et al., 2017).

4.2. Learning and memory impairments after chemokine downregulation

It has been reported that CXCL12 and CXCR4 levels are decreased in patients with AD compared with non-demented controls, supporting a role for this chemokine in memory functioning (Laske et al., 2008). Decreased CXCL12 levels may interfere with proper neuronal signaling and consequently negatively affect memory processing. For instance, in a rat model of temporal lobe epilepsy (TLE), cell proliferation and survival increased when animals were kept in an enriched environment, and this was associated with extended apical dendrites reversing aberrant dendrite development. Moreover, increased expression of CXCL12 and its receptor CXCR4 was accompanied by decreased long-term seizure activity and reduction of the cognitive impairments (Zhang et al., 2015). The same group recently reported that the CXCR4 antagonist AMD3100 reverses the effect of the enriched environment on neurogenesis in TLE rats, but does not abolish the learning improvement (Zhou et al., 2017). They also found that enriched environment combined with AMD3100 suppresses long-term seizure activity. These results suggest that not only this CXCR4 antagonist could be a promising candidate for TLE treatment but also that CXCR4-independent mechanism occurs during learning process (Zhou et al., 2017). We observed memory impairment (both short-term and long-term memory) in *Cxcl12* KD mice in which CXCL12/CXCR4 signaling is reduced. Moreover, we found that also *Cxcr7* KD animals presenting *Cxcr7/Cxcr4/Cxcl12* mRNA reduction, showed memory deficits, supporting the essential role of CXCL12. We confirmed, using the CXCR4 antagonist AMD3100, that acute pharmacological inactivation of CXCR4 causes learning and memory deficits. Similarly, Parachikova and Cotman (2007) reported that AMD3100 impairs object recognition and delays alternation in the T-maze in young adult WT mice. Our data provide further evidence for a role of CXCL12 and its receptors in learning and memory. It represents a potentially new pathway implicated in memory processes, and thus a novel target in learning and memory-related disorders, including neurodegenerative pathologies, such as AD. For instance, in Tg2576 mice that overexpress a mutated amyloid precursor protein, CXCL12 mRNA and protein and CXCR4 are downregulated when learning deficits are detected (Parachikova and Cotman, 2007).

We also found that in *Cxcl12* KD mice, basal levels of *c-Fos*, *Arc* and *Egr1*, three IEGs involved in memory formation, are upregulated. Measures were done 24 h after the last behavioral session, as

animals underwent long term behavioral training, and do only reflect basal levels of IEGs. However, we observed marked differences suggesting that tonic adaptations took place. *Arc* regulates AMPA receptor trafficking as well as long-term potentiation and depression, and its transcription is induced by NMDA receptors (Shepherd and Bear, 2011). Its increased expression in *Cxcl12* KD mice might indicate the activation of neuronal activity through the (alternative) compensatory CXCR7 pathway. *Egr1* regulates genes associated with synaptic plasticity/memory by binding to specific Egr-response elements in genomic DNA sequences (Veyrac et al., 2014), and is involved in activity-dependent neuronal responses. CXCL12/CXCR4 signaling rapidly induces its expression in a concentration-dependent manner (Luo et al., 2008). However, no study yet investigated Egr1 regulation by CXCL12/CXCR7 pathway. Conversely, *Creb1* expression was reduced in both *Cxcl12* KD and *Cxcr7* KD mice. This gene plays a global role in neuronal excitability, synaptic plasticity and memory formation (Lisman et al., 2018). These findings suggest that the CXCL12 chemokine may help to maintain CREB-dependent control of excitability for brain plasticity and memory formation.

4.3. Altered neurogenesis after chemokine downregulation

In the hippocampus, where memory processing is initiated, the detailed analysis of CXCR4/CXCR7/CXCL12 expression profiles indicated that both ligand and receptors are expressed in the different hippocampal cell types throughout life. Hippocampal neurogenesis and memory ability are two hallmarks of brain plasticity in the adult brain, that are inter-related. When both aspects of brain plasticity are examined in mouse models, correlational or causative inter-relationships are sometime difficult to reconcile (see, for instance, Abrous & Wojtowicz, 2015). Regarding the influence of neurogenesis on learning, the role of new hippocampal neurons in memory has been examined in terms of their causal role on learning only recently. In particular, studies showed a marked involvement of neurogenesis in spatial memory. Using a model with selective ablation of neurogenesis by overexpressing Bax in neuronal precursors, Dupret et al. clearly showed that adult-born neurons are required for allocentric, but not egocentric, strategy and the flexible use of acquired spatial information in the water-maze (Dupret et al., 2008). Using brain

irradiation, Madsen et al. observed both blockade of neurogenesis and deficits in delayed alternation in the T-maze, a hippocampus-dependent place-recognition task closely related to spontaneous alternation (Madsen et al., 2003). The relation between neurogenesis and memory is therefore clearly identified for place learning and spatial memory tasks, as involved in water-maze learning and alternation performances. However, the Y-maze test may be less dependent upon neurogenesis since the paradigm involves short-term working memory and several studies showed deconnection between the level of cell proliferation and maturation and performances in the Y-maze (Sakalem et al., 2017). However, since our preliminary experiments identified alternation deficits in the Y-maze for CXCL12 KD and CXCR7 KD mice, we selected both place learning in the water-maze and spontaneous alternation in the Y-maze for behavioral examination of the animals.

In the DG, neural stem cells express CXCR4 and CXCR7, granule cells co-express CXCL12 and CXCR7 (Abe et al., 2018; Banisadr et al., 2015; Tiveron et al., 2010) and hylus interneurons express only CXCR7. Therefore, CXCR7 appears to be expressed in all hippocampal cell types, from neural stem cells to differentiated neurons such as interneurons and granule cells. Conditional knockout models have been used to evaluate CXCR7 role during neurogenesis and positioning of new hippocampal neurons; however, it has only been partially described.

Downregulation of CXCL12 pathways affect differentially neurogenesis in the SGZ of the DG. In *Cxcl12* KD mice, we observed a reduction of Ki67-positive cells, indicating a reduction of proliferating neural stem cells. Conversely, the level of SOX2, a transcription factor expressed in cell progenitors, was not modified. We also confirmed that CXCR4 expression reduction induces proliferation deficits, while CXCR7 might promote survival signals, independently of CXCR4 (Abe et al., 2018; Schultheiß et al., 2013).

In *Cxcr7* KD mice, progenitor proliferation and survival (SOX2-/Ki67-positive progenitors) were comparable to those observed in control animals, while neuron differentiation, measured by DCX expression, was markedly reduced, either at the immature or differentiated stage. Thus, CXCR7/CXCL12 signaling reduction leads to abnormal neuronal commitment of SGZ progenitors, revealing a new CXCR7 role during adult neurogenesis. It was previously reported that CXCR7 is involved in oligodendrocyte

differentiation in the central nervous system (Williams et al., 2014) and controls the migration of several neuron types during embryonic development (Sánchez-Alcañiz et al., 2011; Trousse et al., 2015; Wang et al., 2011). Although the expression of *Cxcr4* and *Cxcr7* was reduced in *Cxcr7* KD mice, we could hypothesize that CXCR7 role in differentiation is distinct from that of CXCR4 on neural progenitor survival during adult neurogenesis (Abe et al., 2018; Schultheiß et al., 2013). Indeed, accumulated evidences in mesenchymal stem cells indicate that CXCR7 regulates not only CXCL12 expression but also induces mesenchymal stem cell differentiation into alveolar cells (Shao et al., 2019; Yuan et al., 2018).

As astrocytes and microglia also express CXCR4 and CXCR7, deregulation of the CXCL12 signaling pathway could affect also glial activation. CXCR7 expression is increased in astrocytes of the cortex of a rat model of stroke and in the hippocampus of patients with in AD, while CXCR4 level is not affected (Puchert et al., 2017). In *Cxcl12* KD mice, we observed an increase in astrocytic/microglial markers that might be linked to the impaired CXCL12 signaling in their brain. CXCL12/CXCR4 signaling reduction in AD models and in patients with AD is associated with impaired learning and memory acquisition. In such contexts, neurotoxicity leads to glial cell activation, cellular elements of the inflammatory response, that is involved in memory defects.

4.4. Concluding remarks

Here, we showed that downregulation of the *Cxcl12* chemokine in mice is accompanied by reduction of *Cxcr4* expression, affects their learning ability, causes glial activation, and deregulates IEG expression and in cell proliferation in the DG. Downregulation of the *Cxcr7* receptor in mice is accompanied by reduction of both *Cxcl12* and *Cxcr4* expression, affects learning, reduces *c-Fos* and *Creb1* levels and impairs cell maturation in the DG. Altogether, these results suggest that the chemokine pathways may therefore play an important role in brain plasticity with CXCL12/CXCR4 and CXCL12/CXCR7 pathway-specific effects on hippocampal neurogenesis, and with major impacts on glial reaction, IEG expression and memory abilities. Their role in neurodegenerative pathologies must be carefully studied.

Funding

This work was supported by INSERM and EPHE funding.

Declaration of interest

None.

Author contributions

G. N., T.M. and M.R. designed research. F.T., J.A., M.S., L.C., E.G., T.M. and M.R. performed research; F.T., T.M. and M.R. analyzed data and wrote the paper.

Acknowledgements

We thank Vicky Diakou from the Imaging facility of the University of Montpellier and Philippe Clair from the qPCR facility of the University of Montpellier. The authors are grateful to Dr Takashi Nagasawa for providing the CXCL12 KD mouse line.

References

Abe, P., Wüst, H.M., Arnold, S.J., van de Pavert, S.A., Stumm, R., 2018. CXCL12-mediated feedback from granule neurons regulates generation and positioning of new neurons in the dentate gyrus. Glia. https://doi.org/10.1002/glia.23324

Ables, J.L., Decarolis, N.A., Johnson, M.A., Rivera, P.D., Gao, Z., Cooper, D.C., Radtke, F., Hsieh, J., Eisch, A.J., 2010. Notch1 is required for maintenance of the reservoir of adult hippocampal stem cells. J. Neurosci. Off. J. Soc. Neurosci. 30, 10484–10492. https://doi.org/10.1523/JNEUROSCI.4721-09.2010

Abrous, D.N., Wojtowicz, J.M., 2015. Interaction between Neurogenesis and Hippocampal Memory System: New Vistas. Cold Spring Harb. Perspect. Biol. 7. https://doi.org/10.1101/cshperspect.a018952

Arancibia, S., Silhol, M., Moulière, F., Meffre, J., Höllinger, I., Maurice, T., Tapia-Arancibia, L., 2008. Protective effect of BDNF against beta-amyloid induced neurotoxicity in vitro and in vivo in rats. Neurobiol. Dis. 31, 316–326. https://doi.org/10.1016/j.nbd.2008.05.012

Banisadr, G., Podojil, J.R., Miller, S.D., Miller, R.J., 2015. Pattern of CXCR7 Gene Expression in Mouse Brain Under Normal and Inflammatory Conditions. J. Neuroimmune Pharmacol. Off. J. Soc. NeuroImmune Pharmacol. https://doi.org/10.1007/s11481-015-9616-y

Chen, Q., Zhang, M., Li, Y., Xu, D., Wang, Y., Song, A., Zhu, B., Huang, Y., Zheng, J.C., 2015. CXCR7 Mediates Neural Progenitor Cells Migration to CXCL12 Independent of CXCR4. Stem Cells Dayt. Ohio. https://doi.org/10.1002/stem.2022

Cheng, X., Wang, H., Zhang, X., Zhao, S., Zhou, Z., Mu, X., Zhao, C., Teng, W., 2017. The Role of SDF-1/CXCR4/CXCR7 in Neuronal Regeneration after Cerebral Ischemia. Front. Neurosci. 11, 590. https://doi.org/10.3389/fnins.2017.00590

Christensen, D.Z., Thomsen, M.S., Mikkelsen, J.D., 2013. Reduced basal and novelty-induced levels of activity-regulated cytoskeleton associated protein (Arc) and c-Fos mRNA in the cerebral cortex and hippocampus of APPswe/PS1ΔE9 transgenic mice. Neurochem. Int. 63, 54–60. https://doi.org/10.1016/j.neuint.2013.04.002

Dupret, D., Revest, J.-M., Koehl, M., Ichas, F., De Giorgi, F., Costet, P., Abrous, D.N., Piazza, P.V., 2008. Spatial relational memory requires hippocampal adult neurogenesis. PloS One 3, e1959. https://doi.org/10.1371/journal.pone.0001959

Guzowski, J.F., Setlow, B., Wagner, E.K., McGaugh, J.L., 2001. Experience-dependent gene expression in the rat hippocampus after spatial learning: a comparison of the immediate-early genes Arc, c-fos, and zif268. J. Neurosci. Off. J. Soc. Neurosci. 21, 5089–5098.

Kilkenny, C., Browne, W.J., Cuthill, I.C., Emerson, M., Altman, D.G., 2010. Improving bioscience research reporting: The ARRIVE guidelines for reporting animal research. J. Pharmacol. Pharmacother. 1, 94–99. https://doi.org/10.4103/0976-500X.72351

Laske, C., Stellos, K., Eschweiler, G.W., Leyhe, T., Gawaz, M., 2008. Decreased CXCL12 (SDF-1) plasma levels in early Alzheimer's disease: a contribution to a deficient hematopoietic brain support? J. Alzheimers Dis. JAD 15, 83–95.

Lieberwirth, C., Pan, Y., Liu, Y., Zhang, Z., Wang, Z., 2016. Hippocampal adult neurogenesis: Its regulation and potential role in spatial learning and memory. Brain Res. 1644, 127–140. https://doi.org/10.1016/j.brainres.2016.05.015

Lisman, J., Cooper, K., Sehgal, M., Silva, A.J., 2018. Memory formation depends on both synapse-specific modifications of synaptic strength and cell-specific increases in excitability. Nat. Neurosci. 21, 309–314. https://doi.org/10.1038/s41593-018-0076-6

Liu, L., Chen, J.-X., Zhang, X.-W., Sun, Q., Yang, L., Liu, A., Hu, S., Guo, F., Liu, S., Huang, Y., Yang, Y., Qiu, H.-B., 2018. Chemokine receptor 7 overexpression promotes mesenchymal stem cell migration and proliferation via secreting Chemokine ligand 12. Sci. Rep. 8, 204. https://doi.org/10.1038/s41598-017-18509-1

Lopez de Armentia, M., Jancic, D., Olivares, R., Alarcon, J.M., Kandel, E.R., Barco, A., 2007. cAMP response element-binding protein-mediated gene expression increases the intrinsic excitability

of CA1 pyramidal neurons. J. Neurosci. Off. J. Soc. Neurosci. 27, 13909–13918. https://doi.org/10.1523/JNEUROSCI.3850-07.2007

Luo, Y., Lathia, J., Mughal, M., Mattson, M.P., 2008. SDF1alpha/CXCR4 signaling, via ERKs and the transcription factor Egr1, induces expression of a 67-kDa form of glutamic acid decarboxylase in embryonic hippocampal neurons. J. Biol. Chem. 283, 24789–24800. https://doi.org/10.1074/jbc.M800649200

Madsen, T.M., Kristjansen, P.E.G., Bolwig, T.G., Wörtwein, G., 2003. Arrested neuronal proliferation and impaired hippocampal function following fractionated brain irradiation in the adult rat. Neuroscience 119, 635–642.

Maurice, T., 2016. Protection by sigma-1 receptor agonists is synergic with donepezil, but not with memantine, in a mouse model of amyloid-induced memory impairments. Behav. Brain Res. 296, 270–278. https://doi.org/10.1016/j.bbr.2015.09.020

Maurice, T., Hiramatsu, M., Itoh, J., Kameyama, T., Hasegawa, T., Nabeshima, T., 1994a. Behavioral evidence for a modulating role of sigma ligands in memory processes. I. Attenuation of dizocilpine (MK-801)-induced amnesia. Brain Res. 647, 44–56.

Maurice, T., Su, T.P., Parish, D.W., Nabeshima, T., Privat, A., 1994b. PRE-084, a sigma selective PCP derivative, attenuates MK-801-induced impairment of learning in mice. Pharmacol. Biochem. Behav. 49, 859–869.

Nadeau, S., Rivest, S., 2000. Role of microglial-derived tumor necrosis factor in mediating CD14 transcription and nuclear factor kappa B activity in the brain during endotoxemia. J. Neurosci. Off. J. Soc. Neurosci. 20, 3456–3468.

Naert, G., Rivest, S., 2011. CC chemokine receptor 2 deficiency aggravates cognitive impairments and amyloid pathology in a transgenic mouse model of Alzheimer's disease. J. Neurosci. Off. J. Soc. Neurosci. 31, 6208–6220. https://doi.org/10.1523/JNEUROSCI.0299-11.2011

Nagasawa, T., Hirota, S., Tachibana, K., Takakura, N., Nishikawa, S., Kitamura, Y., Yoshida, N., Kikutani, H., Kishimoto, T., 1996. Defects of B-cell lymphopoiesis and bone-marrow myelopoiesis in mice lacking the CXC chemokine PBSF/SDF-1. Nature 382, 635–638. https://doi.org/10.1038/382635a0

Nilsson, M., Perfilieva, E., Johansson, U., Orwar, O., Eriksson, P.S., 1999. Enriched environment increases neurogenesis in the adult rat dentate gyrus and improves spatial memory. J. Neurobiol. 39, 569–578.

Parachikova, A., Cotman, C.W., 2007. Reduced CXCL12/CXCR4 results in impaired learning and is downregulated in a mouse model of Alzheimer disease. Neurobiol. Dis. 28, 143–153. https://doi.org/10.1016/j.nbd.2007.07.001

Phan, L.K., Lin, F., LeDuc, C.A., Chung, W.K., Leibel, R.L., 2002. The mouse mahoganoid coat color mutation disrupts a novel C3HC4 RING domain protein. J. Clin. Invest. 110, 1449–1459. https://doi.org/10.1172/JCI16131

Puchert, M., Pelkner, F., Stein, G., Angelov, D.N., Boltze, J., Wagner, D.-C., Odoardi, F., Flügel, A., Streit, W.J., Engele, J., 2017. Astrocytic expression of the CXCL12 receptor, CXCR7/ACKR3 is a hallmark of the diseased, but not developing CNS. Mol. Cell. Neurosci. 85, 105–118. https://doi.org/10.1016/j.mcn.2017.09.001

Raber, J., Rola, R., LeFevour, A., Morhardt, D., Curley, J., Mizumatsu, S., VandenBerg, S.R., Fike, J.R., 2004. Radiation-induced cognitive impairments are associated with changes in indicators of hippocampal neurogenesis. Radiat. Res. 162, 39–47.

Rodríguez Cruz, Y., Strehaiano, M., Rodríguez Obaya, T., García Rodríguez, J.C., Maurice, T., 2017. An Intranasal Formulation of Erythropoietin (Neuro-EPO) Prevents Memory Deficits and Amyloid Toxicity in the APPSwe Transgenic Mouse Model of Alzheimer's Disease. J. Alzheimers Dis. JAD 55, 231–248. https://doi.org/10.3233/JAD-160500

Sakalem, M.E., Seidenbecher, T., Zhang, M., Saffari, R., Kravchenko, M., Wördemann, S., Diederich, K., Schwamborn, J.C., Zhang, W., Ambrée, O., 2017. Environmental enrichment and physical exercise revert behavioral and electrophysiological impairments caused by reduced adult neurogenesis. Hippocampus 27, 36–51. https://doi.org/10.1002/hipo.22669

Sánchez-Alcañiz, J.A., Haege, S., Mueller, W., Pla, R., Mackay, F., Schulz, S., López-Bendito, G., Stumm, R.,

Marín, O., 2011. Cxcr7 Controls Neuronal Migration by Regulating Chemokine Responsiveness. Neuron 69, 77–90. https://doi.org/10.1016/j.neuron.2010.12.006

Schönemeier, B., Kolodziej, A., Schulz, S., Jacobs, S., Hoellt, V., Stumm, R., 2008. Regional and cellular localization of the CXCl12/SDF-1 chemokine receptor CXCR7 in the developing and adult rat brain. J. Comp. Neurol. 510, 207–220. https://doi.org/10.1002/cne.21780

Schultheiß, C., Abe, P., Hoffmann, F., Mueller, W., Kreuder, A.-E., Schütz, D., Haege, S., Redecker, C., Keiner, S., Kannan, S., Claasen, J.-H., Pfrieger, F.W., Stumm, R., 2013. CXCR4 prevents dispersion of granule neuron precursors in the adult dentate gyrus. Hippocampus 23, 1345–1358. https://doi.org/10.1002/hipo.22180

Schwenk, F., Baron, U., Rajewsky, K., 1995. A cre-transgenic mouse strain for the ubiquitous deletion of loxP-flanked gene segments including deletion in germ cells. Nucleic Acids Res. 23, 5080–5081.

Shao, Y., Zhou, F., He, D., Zhang, L., Shen, J., 2019. Overexpression of CXCR7 promotes mesenchymal stem cells to repair phosgene-induced acute lung injury in rats. Biomed. Pharmacother. Biomedecine Pharmacother. 109, 1233–1239. https://doi.org/10.1016/j.biopha.2018.10.108

Shepherd, J.D., Bear, M.F., 2011. New views of Arc, a master regulator of synaptic plasticity. Nat. Neurosci. 14, 279–284. https://doi.org/10.1038/nn.2708

Shimizu, S., Brown, M., Sengupta, R., Penfold, M.E., Meucci, O., 2011. CXCR7 Protein Expression in Human Adult Brain and Differentiated Neurons. PLOS ONE 6, e20680. https://doi.org/10.1371/journal.pone.0020680

Stumm, R.K., Zhou, C., Ara, T., Lazarini, F., Dubois-Dalcq, M., Nagasawa, T., Hollt, V., Schulz, S., 2003. CXCR4 regulates interneuron migration in the developing neocortex. J Neurosci 23, 5123–30.

Tiveron, M.-C., Boutin, C., Daou, P., Moepps, B., Cremer, H., 2010. Expression and function of CXCR7 in the mouse forebrain. J. Neuroimmunol. 224, 72–79.

Trouche, S., Bontempi, B., Roullet, P., Rampon, C., 2009. Recruitment of adult-generated neurons into functional hippocampal networks contributes to updating and strengthening of spatial memory. Proc. Natl. Acad. Sci. U. S. A. 106, 5919–5924. https://doi.org/10.1073/pnas.0811054106

Trousse, F., Poluch, S., Pierani, A., Dutriaux, A., Bock, H.H., Nagasawa, T., Verdier, J.-M., Rossel, M., 2015. CXCR7 Receptor Controls the Maintenance of Subpial Positioning of Cajal–Retzius Cells. Cereb. Cortex 25, 3446–3457. https://doi.org/10.1093/cercor/bhu164

Tzingounis, A.V., Nicoll, R.A., 2006. Arc/Arg3.1: linking gene expression to synaptic plasticity and memory. Neuron 52, 403–407. https://doi.org/10.1016/j.neuron.2006.10.016

van Praag, H., Shubert, T., Zhao, C., Gage, F.H., 2005. Exercise enhances learning and hippocampal neurogenesis in aged mice. J. Neurosci. Off. J. Soc. Neurosci. 25, 8680–8685. https://doi.org/10.1523/JNEUROSCI.1731-05.2005

Veyrac, A., Besnard, A., Caboche, J., Davis, S., Laroche, S., 2014. The transcription factor Zif268/Egr1, brain plasticity, and memory. Prog. Mol. Biol. Transl. Sci. 122, 89–129. https://doi.org/10.1016/B978-0-12-420170-5.00004-0

von Bohlen und Halbach, O., 2011. Immunohistological markers for proliferative events, gliogenesis, and neurogenesis within the adult hippocampus. Cell Tissue Res. 345, 1–19. https://doi.org/10.1007/s00441-011-1196-4

Wang, Y., Li, G., Stanco, A., Long, J.E., Crawford, D., Potter, G.B., Pleasure, S.J., Behrens, T., Rubenstein, J.L.R., 2011. CXCR4 and CXCR7 have distinct functions in regulating interneuron migration. Neuron 69, 61–76. https://doi.org/10.1016/j.neuron.2010.12.005

Wang, Y., Xu, P., Qiu, L., Zhang, M., Huang, Y., Zheng, J.C., 2016. CXCR7 participates in CXCL12 mediated cell cycle and proliferation regulation in mouse neural progenitor cells. Curr. Mol. Med.

Williams, J.L., Patel, J.R., Daniels, B.P., Klein, R.S., 2014. Targeting CXCR7/ACKR3 as a therapeutic strategy to promote remyelination in the adult central nervous system. J. Exp. Med. 211, 791–799. https://doi.org/10.1084/jem.20131224

Yuan, F., Chang, S., Luo, L., Li, Y., Wang, L., Song, Y., Qu, M., Zhang, Z., Yang, G.-Y., Wang, Y., 2018. cxcl12 gene engineered endothelial progenitor cells further improve the functions of oligodendrocyte precursor cells. Exp. Cell Res. 367, 222–231. https://doi.org/10.1016/j.yexcr.2018.03.040

Zhang, X., Liu, T., Zhou, Z., Mu, X., Song, C., Xiao, T., Zhao, M., Zhao, C., 2015. Enriched Environment

Altered Aberrant Hippocampal Neurogenesis and Improved Long-Term Consequences After Temporal Lobe Epilepsy in Adult Rats. J. Mol. Neurosci. MN 56, 409–421. https://doi.org/10.1007/s12031-015-0571-0

Zhou, Z., Liu, T., Sun, X., Mu, X., Zhu, G., Xiao, T., Zhao, M., Zhao, C., 2017. CXCR4 antagonist AMD3100 reverses the neurogenesis promoted by enriched environment and suppresses long-term seizure activity in adult rats of temporal lobe epilepsy. Behav. Brain Res. 322, 83–91. https://doi.org/10.1016/j.bbr.2017.01.014

Legends for the Figures

Figure 1. Experimental protocols: (a) Spontaneous alternation in the Y-maze test (YMT) was tested in a first cohort of *Cxcl12* KD and *Cxcr7* KD mice and their WT littermates (C57BL/6J strain), and the day after they were sacrificed for molecular biology and immunohistochemical analyses. (b) Spontaneous alternation in the Y-maze test (YMT) and place learning in the water-maze test (WMT) were tested in *Cxcl12* KD, *Cxcr7* KD mice and WT littermates (second cohort). Specifically, after the YMT, mice rested for one day and then underwent 5 days of training (Tg) for the WMT (3 swims/day), followed by a retention probe test (Ret) performed 24 h after the last training session. Animals were sacrificed 24h after the last behavioral session, for molecular biology and immunohistochemical analyses. (c) Male Swiss CD-1 mice were treated with the CXCR4 antagonist AMD3100 (1, 3 mg/kg IP) for 4 days. The YMT and step-through passive avoidance (STPA) training were performed 20 min after the drug injection (at day 3 and 4, respectively). Passive avoidance retention was measured 24 h after the training session (day 5).

Figure 2. Expression levels of *Cxcl12, Cxcr7* and *Cxcr4* in hippocampus homogenates of (a) *Cxcl12* KD and (b) *Cxcr7* KD mice; mRNA levels were corrected to *Actb* mRNA levels for each sample (n = 11 *Cxcl12* KD and n = 5 WT littermates; and n= 11 *Cxcr7* KD, n = 8 WT littermates).*** $p<0.001$, ** $p < 0.01$ (unpaired Student's *t*-test).

Figure 3. Learning and memory in *Cxcl12* KD mice: spontaneous alternation in the Y-maze (a, b) and place learning in the water-maze (c-h). Male (M) and female (F) WT littermates (WT) and *Cxcl12* KD (KD) mice were tested in parallel. (a) Spontaneous alternation and (b) number of arm entries in the Y-maze; (c, d) acquisition profiles in the water-maze, (e) acquisition slopes, (f) swimming speed, and (g) presence in the training (T) or other (O) quadrants during the probe test. (h) Acquisition slopes during the working memory test. Data are the mean ± SEM. Two-way ANOVA: $F_{(1,50)} = 15.5$, $p < 0.001$ for genotype, $F < 1$ for sex and interaction, n = 11-18 per group in (a); $F_{(1,50)} = 13.7$, $p < 0.001$ for sex, $F < 1$ for genotype and

interaction in (b); $F_{(1,27)}$ = 5.86, p < 0.05 for genotype, $F_{(1,27)}$ = 1.14, p > 0.05 for sex, F < 1 for interaction in (e); $F_{(1,27)}$ = 23.6, p < 0.0001 for genotype, $F_{(1,27)}$ = 1.80, p > 0.05 for sex, $F_{(1,27)}$ = 1.29, p > 0.05 for interaction in (f); $F_{(1,9)}$ = 5.13, p < 0.05 for genotype, F < 1 for sex and interaction, n = 2-5 in (h). Friedman's repeated-measure ANOVA: Fr = 13.2, p < 0.05, n = 5, for the M-WT group; Fr = 9.98, p < 0.05, n = 11, for the M-KD group in (c); Fr = 18.4, p < 0.001, n = 7, for the F-WT group, Fr = 13.9, p < 0.01, n = 8, for the F-KD group in (d). *p < 0.05, **p < 0.01 vs. the respective WT group; Student's t-test in (a, b, e, f, h). °p < 0.05, °°p < 0.01 *vs*. chance level (15 s); one-sample t-test in (g).

Figure 4. Learning and memory in *Cxcr7* KD mice: spontaneous alternation in the Y-maze (a, b) and place learning in the water-maze (c-h). Male (M) and female (F) WT littermates (WT) and *Cxcr7* KD (KD) mice were tested in parallel. (a) Spontaneous alternation and (b) number of arm entries in the Y-maze; (c, d) acquisition profiles in the water-maze, (e) acquisition slopes, (f) swimming speed, and (g) presence in the training (T) or other (O) quadrants during the probe test. (h) Acquisition slopes during the working memory test. Data are the mean ± SEM. Two-way ANOVA: $F_{(1,52)}$ = 13.2, p < 0.001 for genotype, $F_{(1,52)}$ = 1.54, p > 0.05, for sex, F <1 for interaction, n = 12-15 per group in (a); $F_{(1,52)}$ = 4.26, p < 0.05 for sex, $F_{(1,52)}$ = 2.56, p > 0.05, for genotype, $F_{(1,52)}$ = 1.87, p > 0.05, for interaction in (b); F < 1 for genotype, sex and interaction in (e); F <1 for genotype, sex and interaction in (f); $F_{(1,26)}$ = 5.79, p < 0.05 for genotype, F <1 for sex and interaction, n = 5-10 in (h). Friedman's repeated-measure ANOVA: Fr = 17.7, p < 0.01, n = 5 for the M-WT group; Fr = 18.4, p < 0.001, n = 10, for the M-KD group in (c); Fr = 17.7, p <0.01, n = 5, for the F-WT group, Fr = 23.0, p < 0.0001, n = 10, for the F-KD group in (d). *p < 0.05, **p < 0.01 vs. the respective WT group; Student's t-test in (a, b, e, f, h). °p <0.05 *vs*. chance level (15 s); one-sample t-test in (g).

Figure 5. AMD3100 effect on learning and memory in mice (see Fig. 1c for the experimental protocol): (a) spontaneous alternation and (b) number of arm entries in the Y-maze; (c) step-through latency and (d) escape latency in the passive avoidance test. Data are the mean ± SEM in (a, b) and median and

interquartile range in (c, d). ANOVA: $F_{(2,27)} = 3.55$, $p < 0.05$, n = 9-10 per group in (a), $F < 1$ in (b). Kruskal-Wallis non-parametric ANOVA: $H = 8.42$, $p < 0.05$, n = 10 per group in (c), $H = 3.67$, $p > 0.05$ in (d). *$p <$ 0.05, **$p < 0.01$ vs. the V-treated group; Dunnett's test in (a); Dunn's test in (c).

Figure 6. Expressions of early genes involved in memory and learning are affected after *Cxcl12* and *Cxcr7* KD. RT-qPCR of *c-Fos*, *Arc*, *Egr1* and *Creb1* in the hippocampus of: (a) *Cxcl12* KD mice and (b) *Cxcr7* KD mice. Values were normalized to the expression of actin, determined in triplicate within each experiment, in four independent experiments with n = 5 *Cxcl12* WT, n = 11 *Cxcl12* KD, n = 8 *Cxcr7* WT, and n = 11 *Cxcr7* KD in total. * $p < 0.05$, ** $p < 0.01$, *** $p < 0.001$; unpaired Student *t*-test.

Figure 7. Neurogenesis is differentially impaired in *Cxcl12* and *Cxcr7* KD mice. (a-l') Coronal sections with magnifications in insets showing Ki67 (a-b'; g-h'), SOX2 (c-d'; i-j'), and DCX (e-f; k-l') localization in the hippocampal DG by immunohistochemistry analysis. (a-f; m') The number of progenitors in DG is decreased in *Cxcl12* KD mice compared with WT littermates. (g-l'; o). The number of newborn neurons is decreased in DG of *Cxcr7* KD mice compared with WT littermates. (m-o) Quantification of Ki67- (m), SOX2- (n) and DCX-positive cells (o) in DG. (n) The total number of SOX2-positive cells was unchanged in the DG of *Cxcl12* KD and *Cxcr7* KD mice compared with WT littermates. Data represent the mean ± SEM, groups were compared using the unpaired *t*-test (m-o). The number of KD and WT mice is indicated in each histogram in (m). Scale bars = 100 µm in (a-l), 40 µm in (a'-l'). *$p < 0.05$.

Figure 8. In *Cxcl12* KD mice, microglia in the hippocampal DG is increased. (a-h') Representative images of GFAP and IBA-1 expression in *Cxcl12* KD and *Cxcr7* KD mice and the respective WT littermates by immunohistochemistry analysis. (a-b'; e-f') GFAP labeling of WT, *Cxcl12* KD and *Cxcr7* KD mice. (c-d'; g-h') IBA-1 labeling of WT, *Cxcl12* KD and *Cxcr7* KD mice. Quantification of: (i) GFAP and (j) IBA-1 staining intensity in the DG. The number of mice per group is indicated within the columns in (i,j). Scale bars = 100 µm in (a-h), 50 µm in (a'-h'). *$p < 0.05$; Mann-Whitney's test.

Supplementary Materials

Supplementary Table

Supplementary Table 1. Primers used for qPCR assays

Gene	Forward primer	Reverse primer
Cxcr7	TGT CCC GCC ATG CCC AAC AA	TGC ACG AGA CTG ACC ACC CAG A
Cxcr4	TTG CCA TTG TCC ACG CCA CCA	TCT TGA GGG CCT TGC GCT TCT
Cxcl12	CCT GAG GAA GGC TGA CCT CCG T	AGC TCC ATT GTG CAC GGG CG
Creb1	CTA GTG CCC AGC AAC CAA GT	GGA GGA CGC CAT AAC AAC TC
c-Fos	CGG GTT TCA ACG CCG ACT A	TTG GCA CTA GAG ACG GAC AGA
Arc	AGG GTG AAC CAC TCG ACC AGT	TCT GGT ACA GGT CCC GCT TG
Egr1	AGC ACC TGA CCA CAG AGT	CCT TCT CAT TAT TCA GAG CGA
Actb	GCA AGC AGG AGT ACG ATG AG	AGG GTG TAA AAC GCA GCT C

Legends to Supplementary Figures

Supplementary Figure 1. In *Cxcr7* KD mice, progenitor cells in the GCL are increased and differentiation of newborn neurons is affected. (a) Quantification of SOX2-positive cells (j) in the GCL relative to the total number of SOX2-positive cells in SGZ and GCL showed an increase the percentage of progenitors in GCL of *Cxcr7* KD mice compared with WT littermates. (b) Quantification of DCX-positive neuroblasts and immature neurons/mm^2 showed a decrease the number of these two subpopulations in *Cxcr7* KD mice compared to WT littermates. (c) Quantification of DCX-positive neuroblasts and immature neurons relative to the total number of DCX-positive cells showed an increase in the number of neuroblasts to the detriment of immature neurons in *Cxcr7* KD mice compared with WT mice. Data are the mean ± SEM, groups were compared using the unpaired Student's *t* test (*$p < 0.05$). The number of mice per group is indicated in the columns.

Supplementary Figure 2. In *Cxcr7* KD mice, the number of immature neurons is decreased and dendrite growth is reduced. (a-d') Hippocampus sections were immunostained for DCX (red) and stained with DAPI (blue; nuclei) and images acquired by confocal microscopy. (a-a') In WT mice, there is high density of DCX-positive immature neurons in GCL. (b-b') In *Cxcr7* KD mice, the number and morphology of DCX-positive cells are affected. Image stack analysis demonstrated a reduction in the number of DCX-positive immature neurons and of outgrowing dendrites of DCX-positive neurons in the GCL. (c-d') No difference is observed in *Cxcl12* KD mice compared with WT littermates. Abbreviation: GCL, granule cell layer. Scale bar = 50 µm.

Figure 1

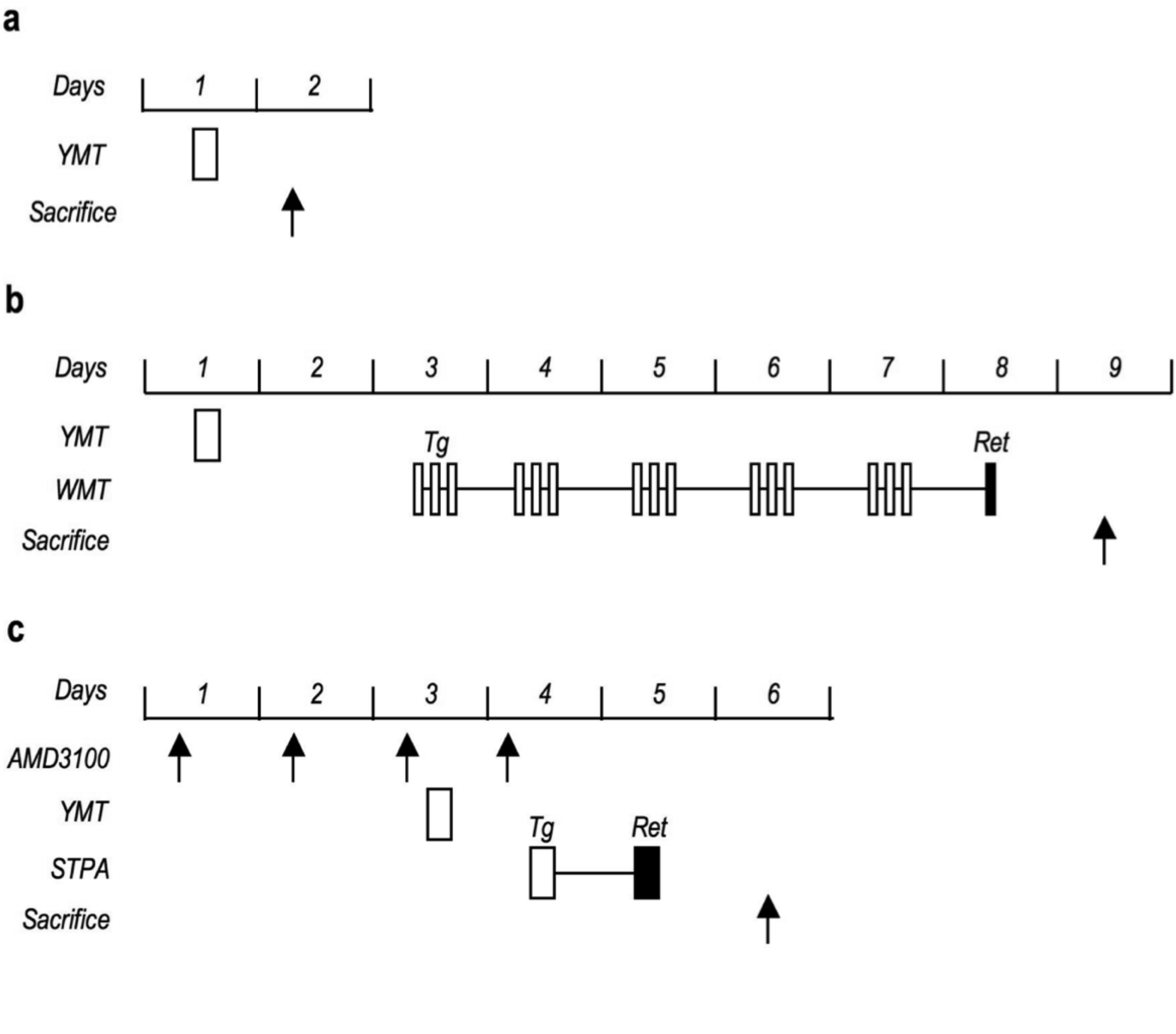
a
Days
1
2
YMT
Sacrifice
b
Days
1
2
3
4
5
6
7
8
9
YMT
Tg
Ret
WMT
Sacrifice
c
Days
1
2
3
4
5
6
AMD3100
YMT
Tg
Ret
STPA
Sacrifice

Figure 2

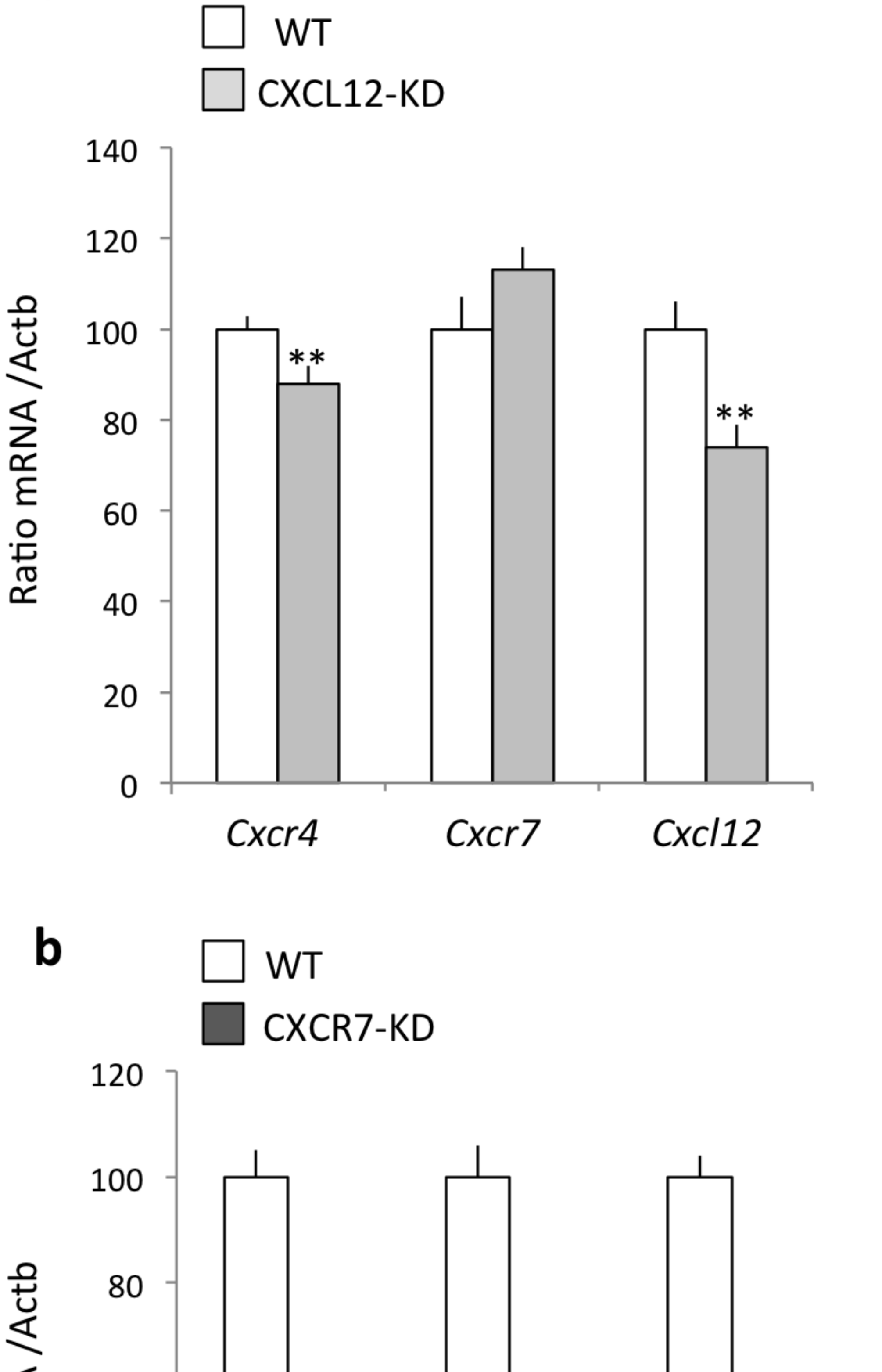
a
WT
CXCL12-KD
Ratio mRNA /Actb
140
120
100
80
60
40
20
0
**
**
Cxcr4
Cxcr7
Cxcl12
b
WT
CXCR7-KD
Ratio mRNA /Actb
120
100
80
60
40
20
0
***
***
***
Cxcr4
Cxcr7
Cxcl12

Figure 3

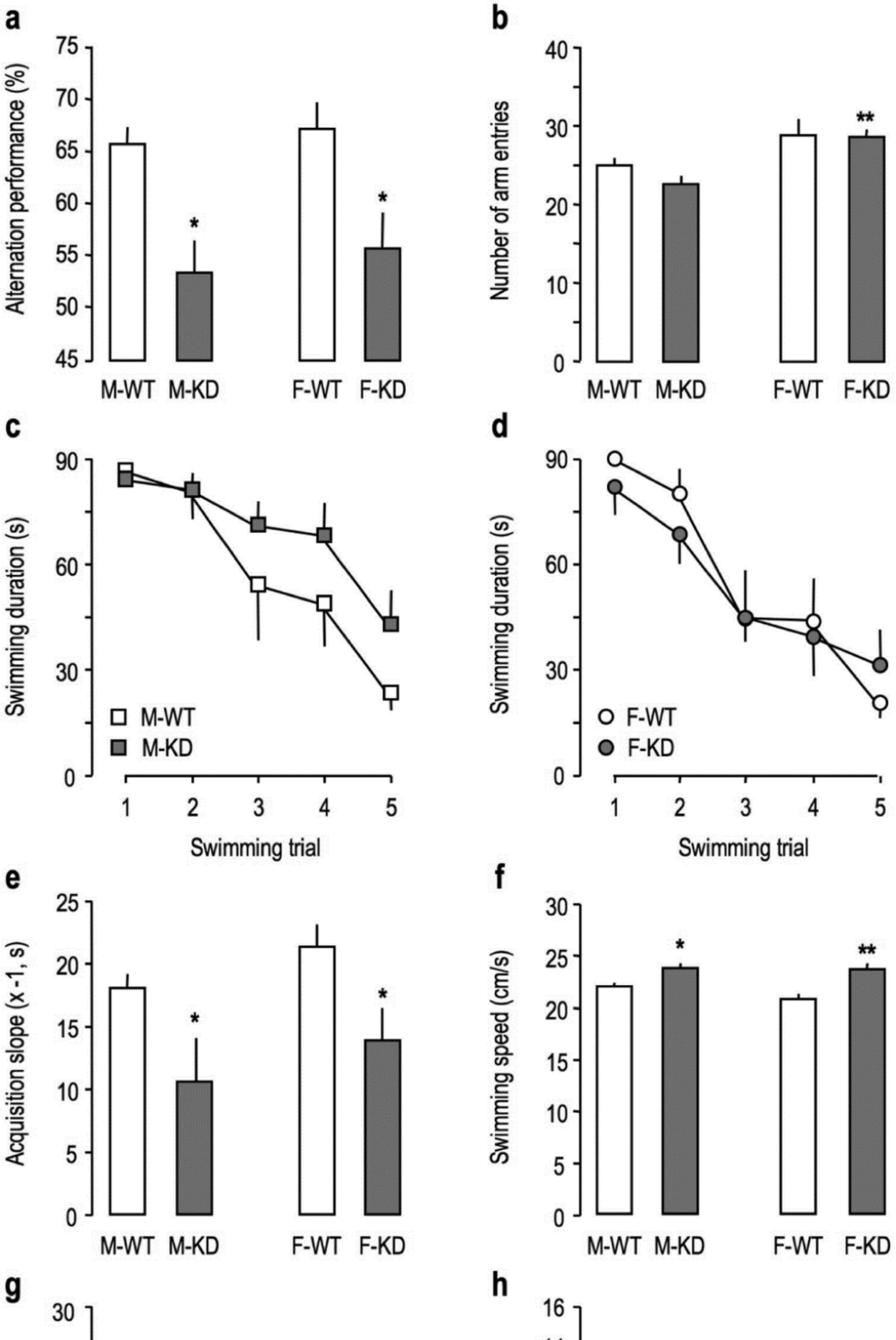
a
Alternation performance (%)
75
70
65
60
55
50
45
*
*
M-WT
M-KD
F-WT
F-KD
b
Number of arm entries
40
30
20
10
0
**
M-WT
M-KD
F-WT
F-KD
c
Swimming duration (s)
90
60
30
0
M-WT
M-KD
1
2
3
4
5
Swimming trial
d
Swimming duration (s)
90
60
30
0
F-WT
F-KD
1
2
3
4
5
Swimming trial
e
Acquisition slope (x -1, s)
25
20
15
10
5
0
*
*
M-WT
M-KD
F-WT
F-KD
f
Swimming speed (cm/s)
30
25
20
15
10
5
0
*
**
M-WT
M-KD
F-WT
F-KD
g
Presence in quadrant (s)
30
25
20
15
10
5
0
°
°°
T
O
T
O
T
O
T
O
M-WT
M-KD
F-WT
F-KD
h
Working memory test acquisition slope (x-1, s)
16
14
12
10
8
6
4
2
0
*
*
M-WT
M-KD
F-WT
F-KD

Figure 4

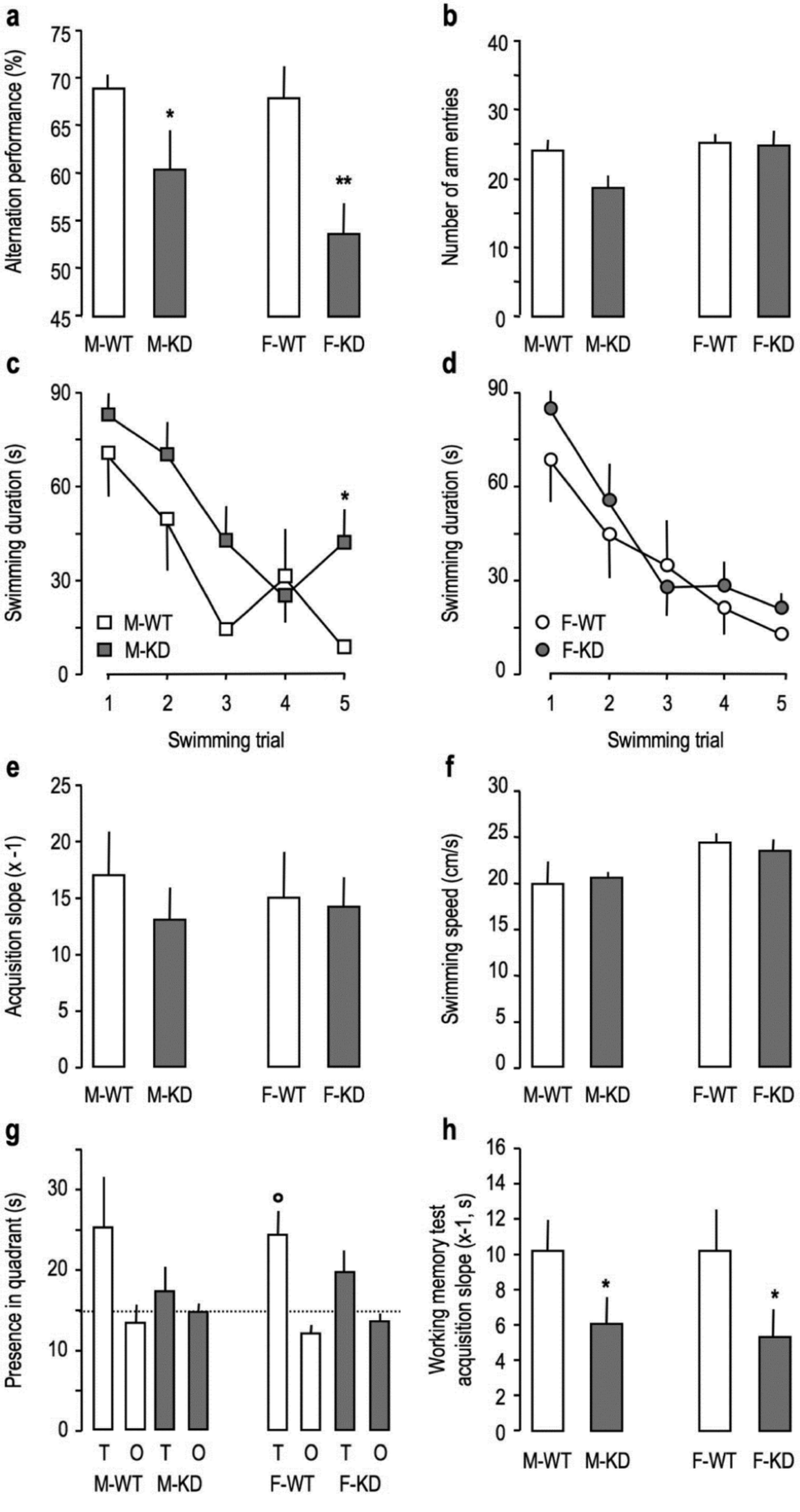
a
Alternation performance (%)
75
70
65
60
55
50
45
*
**
M-WT
M-KD
F-WT
F-KD
b
Number of arm entries
40
30
20
10
0
M-WT
M-KD
F-WT
F-KD
c
Swimming duration (s)
90
60
30
0
M-WT
M-KD
*
1
2
3
4
5
Swimming trial
d
Swimming duration (s)
90
60
30
0
F-WT
F-KD
1
2
3
4
5
Swimming trial
e
Acquisition slope (x -1)
25
20
15
10
5
0
M-WT
M-KD
F-WT
F-KD
f
Swimming speed (cm/s)
30
25
20
15
10
5
0
M-WT
M-KD
F-WT
F-KD
g
Presence in quadrant (s)
30
20
10
0
o
T
O
T
O
M-WT
M-KD
T
O
T
O
F-WT
F-KD
h
Working memory test acquisition slope (x-1, s)
16
14
12
10
8
6
4
2
0
*
*
M-WT
M-KD
F-WT
F-KD

Figure 5

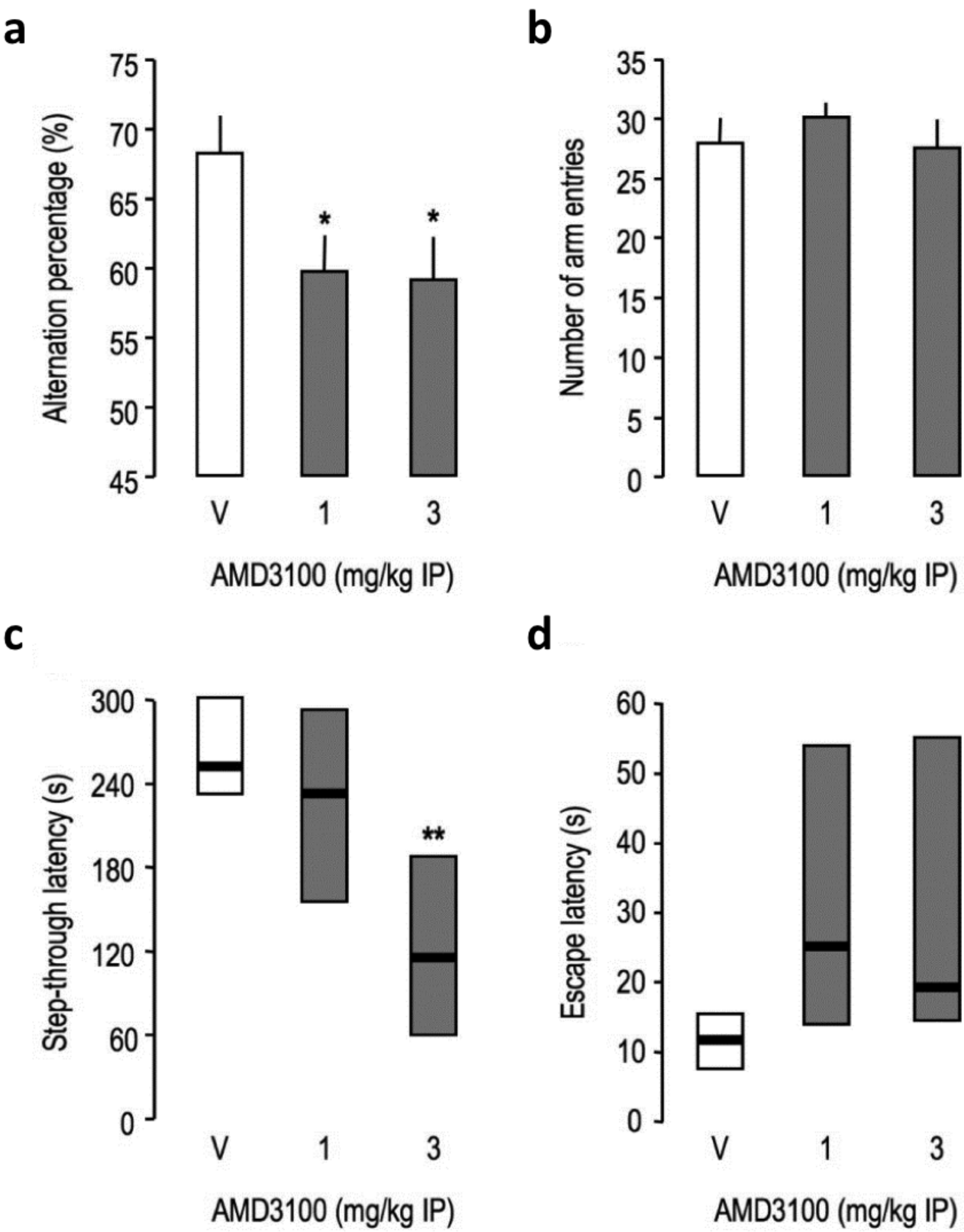
a
Alternation percentage (%)
75
70
65
60
55
50
45
*
*
V
1
3
AMD3100 (mg/kg IP)
b
Number of arm entries
35
30
25
20
15
10
5
0
V
1
3
AMD3100 (mg/kg IP)
c
Step-through latency (s)
300
240
180
120
60
0
**
V
1
3
AMD3100 (mg/kg IP)
d
Escape latency (s)
60
50
40
30
20
10
0
V
1
3
AMD3100 (mg/kg IP)

Figure 6

a

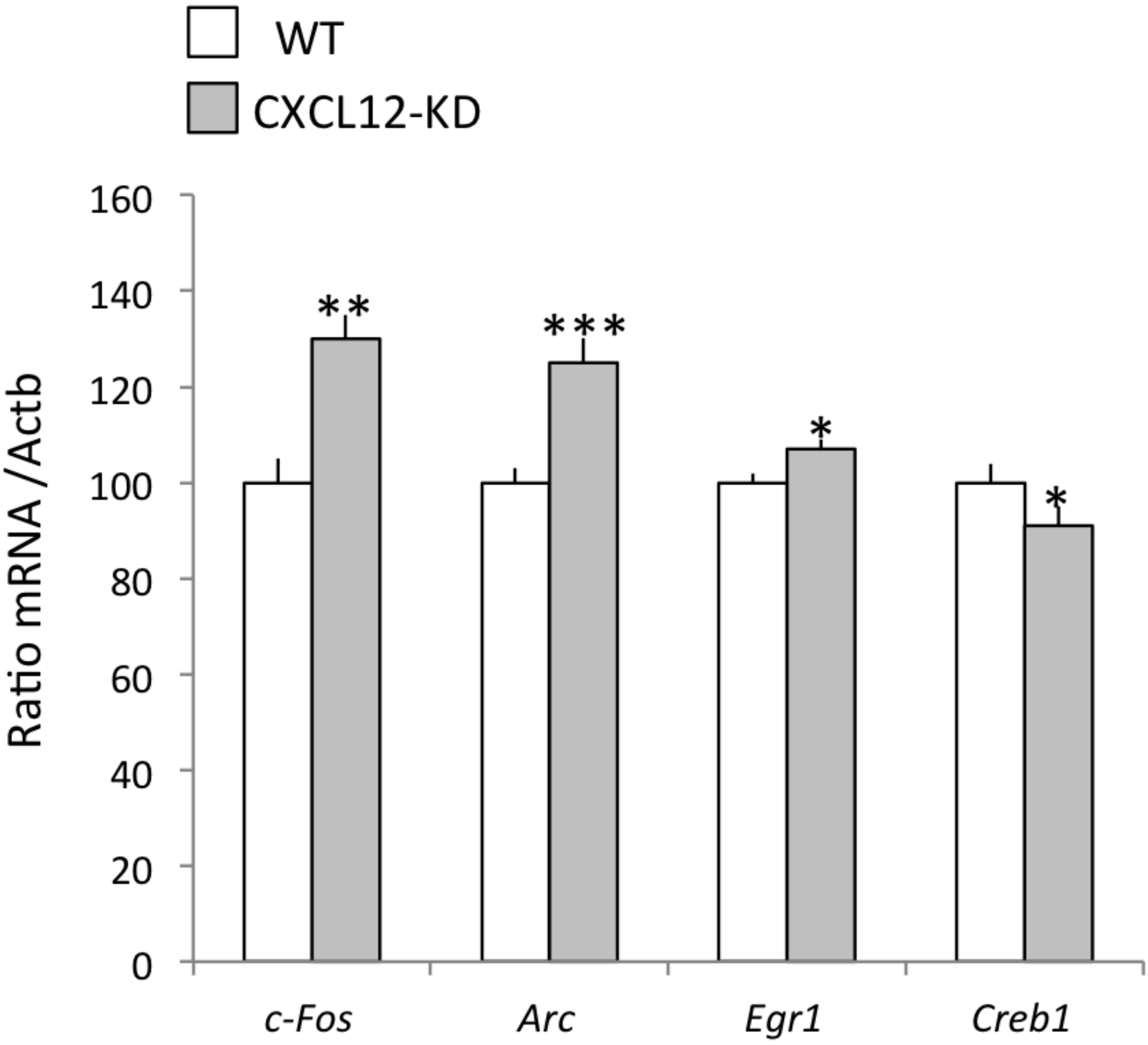
WT
CXCL12-KD
Ratio mRNA /Actb
160
140
120
100
80
60
40
20
0
**
***
*
*
c-Fos
Arc
Egr1
Creb1

b

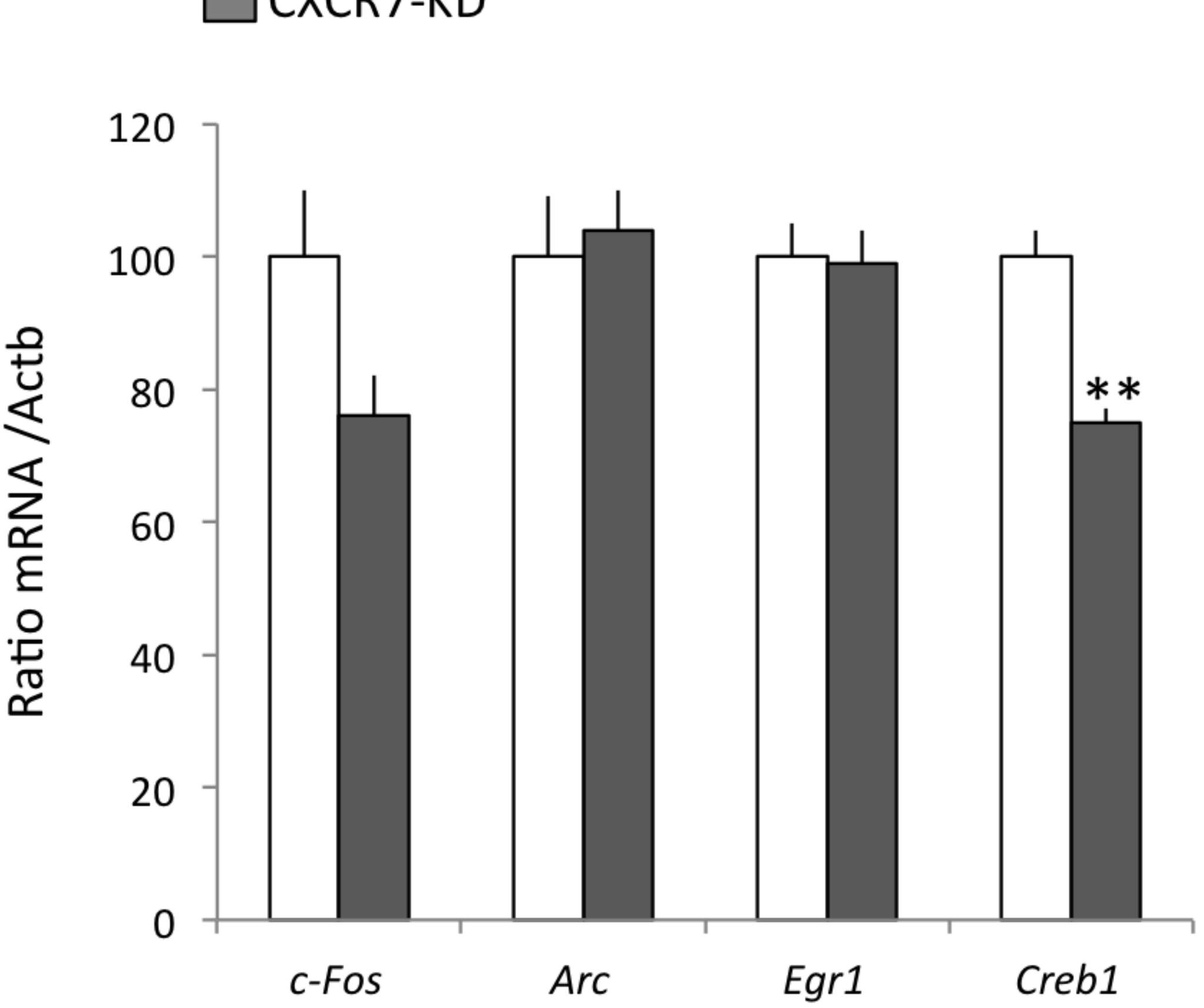
WT
CXCR7-KD
Ratio mRNA /Actb
120
100
80
60
40
20
0
**
c-Fos
Arc
Egr1
Creb1

Figure 7

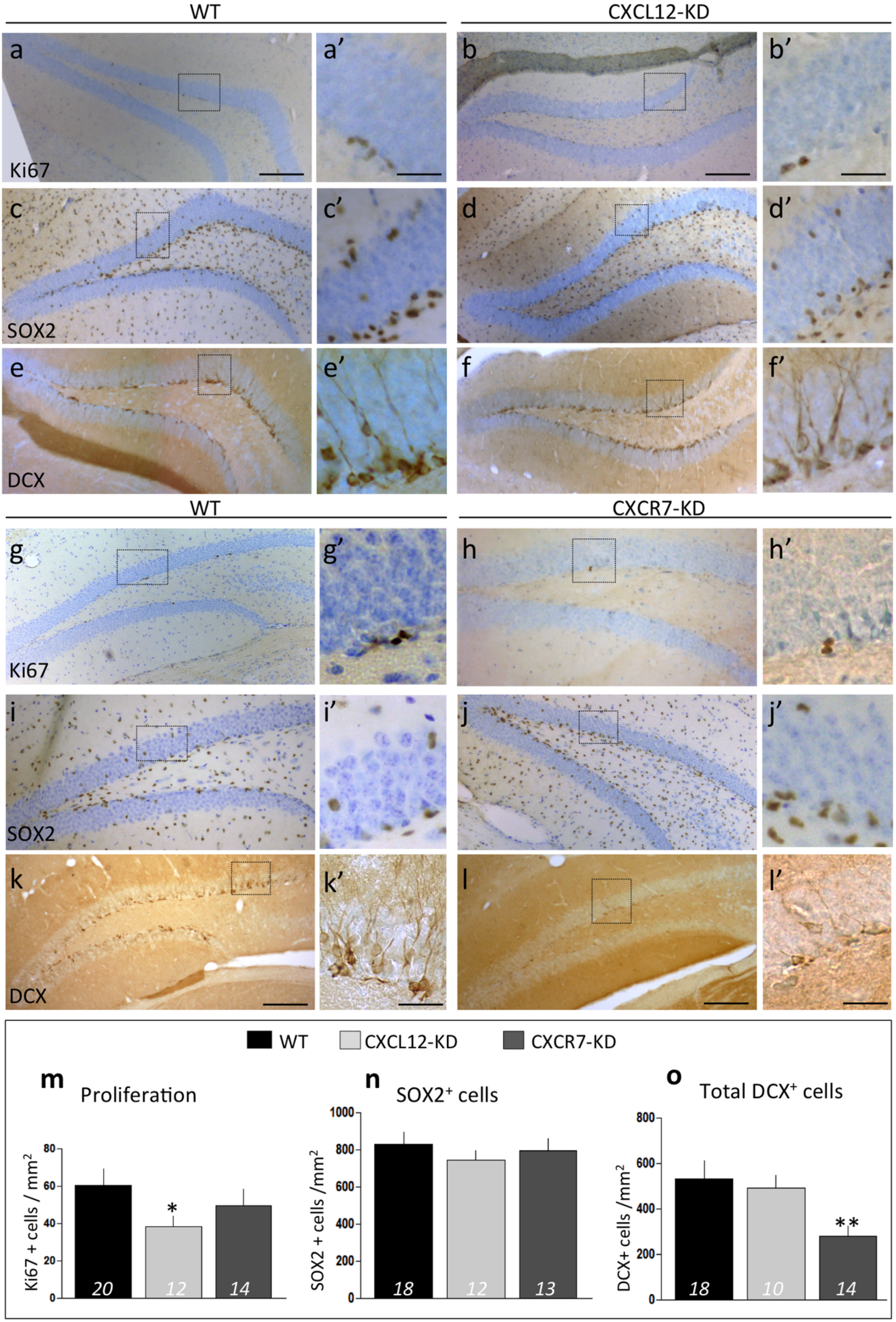
WT
CXCL12-KD
a
a'
b
b'
Ki67
c
c'
d
d'
SOX2
e
e'
f
f'
DCX
WT
CXCR7-KD
g
g'
h
h'
Ki67
i
i'
j
j'
SOX2
k
k'
l
l'
DCX
WT
CXCL12-KD
CXCR7-KD
m
Proliferation
Ki67 + cells / mm2
80
60
40
20
0
*
20
12
14
n
SOX2+ cells
SOX2 + cells /mm2
1000
800
600
400
200
0
18
12
13
o
Total DCX+ cells
DCX+ cells /mm2
800
600
400
200
0
**
18
10
14

Figure 8

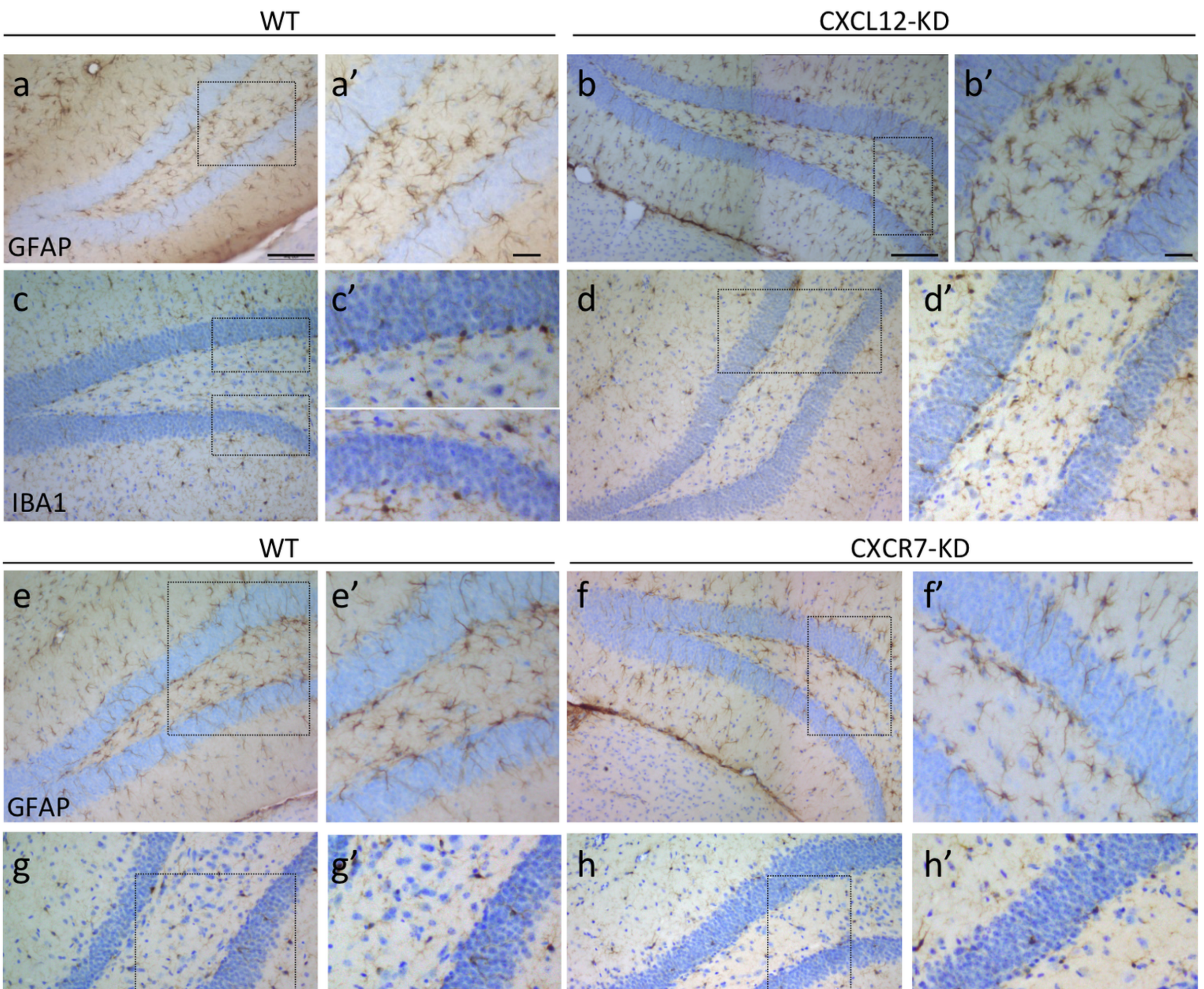
WT
CXCL12-KD
a
a'
b
b'
GFAP
c
c'
d
d'
IBA1
WT
CXCR7-KD
e
e'
f
f'
GFAP
g
g'
h
h'
IBA1

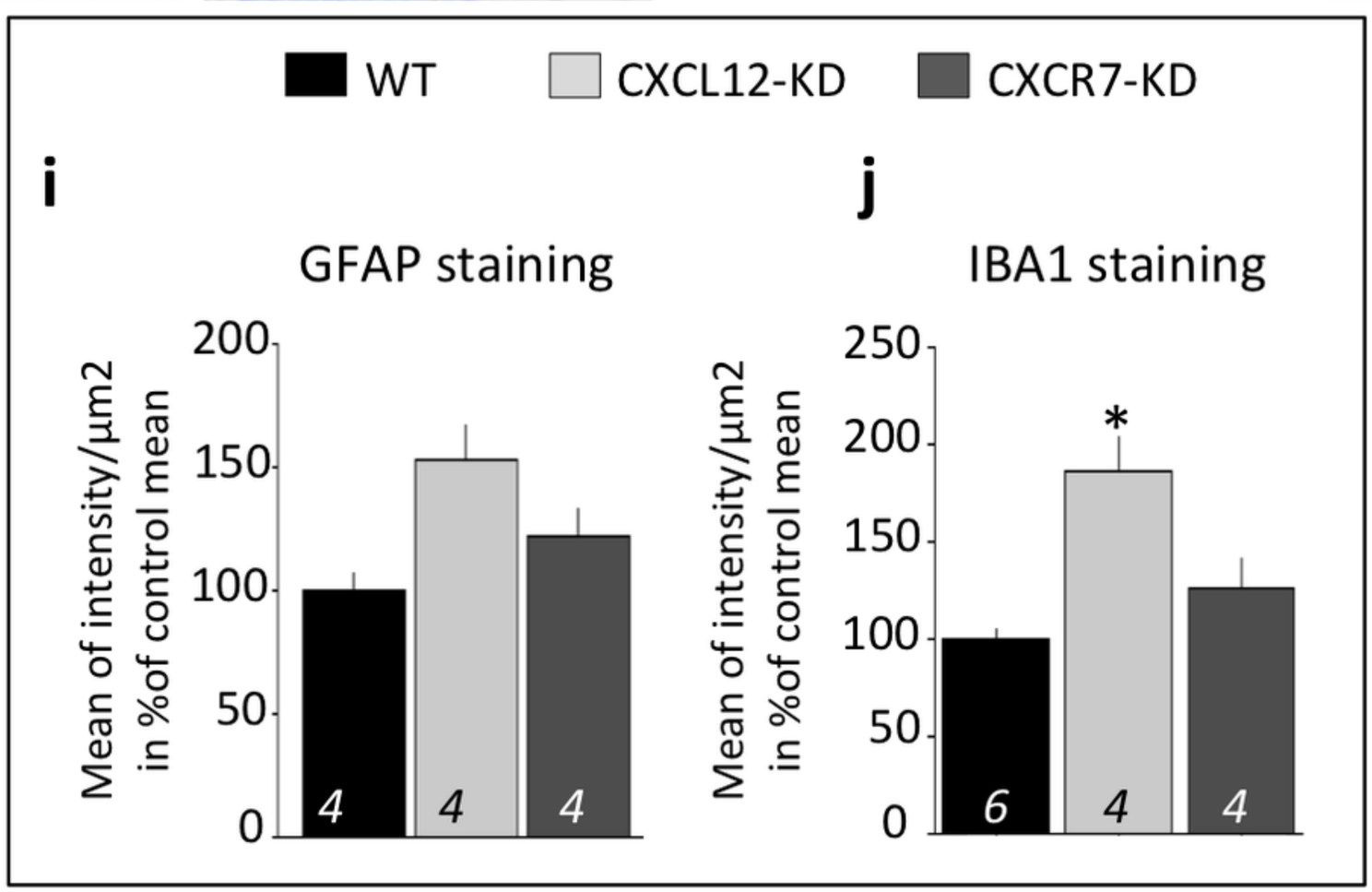
WT
CXCL12-KD
CXCR7-KD
i
GFAP staining
Mean of intensity/µm2 in %of control mean
200
150
100
50
0
4
4
4
j
IBA1 staining
Mean of intensity/µm2 in %of control mean
250
200
150
100
50
0
*
6
4
4

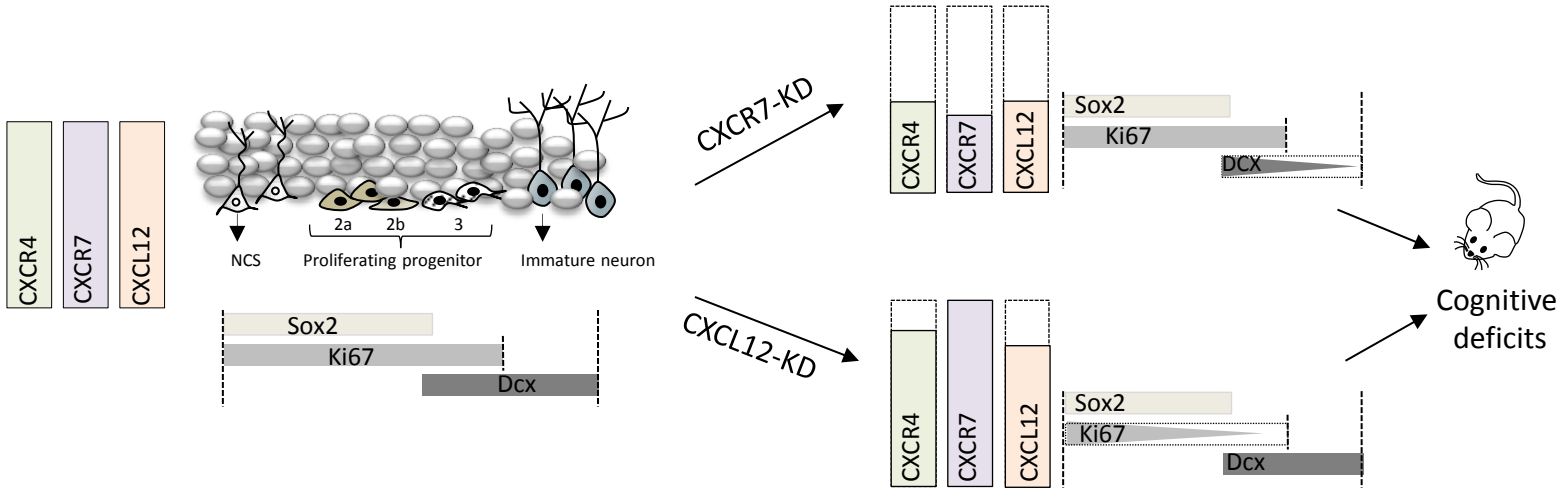
CXCR4
CXCR7
CXCL12
2a
2b
3
NCS
Proliferating progenitor
Immature neuron
Sox2
Ki67
Dcx
CXCR7-KD
CXCL12-KD
Sox2
Ki67
DCX
Sox2
Ki67
Dcx
Cognitive deficits